Heliyon 8 (2022) e09145

Contents lists available at ScienceDirect

Heliyon

journal homepage: www.cell.com/heliyon

Research article

Novel antibacterial hydrogels based on gelatin/polyvinyl-alcohol and graphene oxide/silver nanoconjugates: formulation, characterization, and preliminary biocompatibility evaluation

Jorge Luis Patarroyo [a], Javier Cifuentes [b], Laura N. Muñoz [a], Juan C. Cruz [b,**], Luis H. Reyes [a,*]

[a] Grupo de Diseño de Productos y Procesos (GDPP), Department of Chemical and Food Engineering, Universidad de Los Andes, Bogotá, 111711, Colombia
[b] Department of Biomedical Engineering, Universidad de Los Andes, Bogotá, 111711, Colombia

ARTICLE INFO

Keywords:
Topical treatment
Skin infection
Encapsulation
Graphene oxide
Ag nanoparticles
Antimicrobial activity

ABSTRACT

Antibiotic resistance has become a major public health problem generated by their excessive and inappropriate use. This is worrisome because multiple microbial infections that could traditionally be treated without major complications are now considerably challenging to treat. In this regard, research in this field has been focused on searching for new molecules capable of arresting these microbial infections with high effectiveness, including antimicrobial peptides (AMP) and various nanomaterials. Here, we proposed a novel topical hydrogel treatment based on a polymeric network of gelatin-polyvinyl alcohol-hyaluronic acid encapsulating a graphene oxide (GO) nanoconjugate on which silver nanoparticles (Ag NPs) have been grown. This treatment is intended to be stable, biocompatible, non-toxic, pleasant to skin contact, provide bioavailability of the active agent for a prolonged period in the affected skin area where its application is required and inhibit microbial growth effectively. The nanocomposite hydrogels were characterized in terms of microstructure, thermal resistance, rheological behavior, particle size distribution, texture profile and physical stability, as well as a one-month accelerated stability study. The satisfactory results in terms of physical chemistry, stability on storage modulus (G'), TSI values, and microstructure allowed choosing some points of the experimental design to encapsulate the GO-Ag NPs nanoconjugates. The biological evaluation of these nanocomposites showed that the treatments are biocompatible as they have a very low hemolytic effect (less than 5%) and a moderate platelet aggregating capacity (35%–45%). Finally, 100% of bacterial growth was inhibited by the action of the topical nanocomposite hydrogel treatments. These results led to affirm that these treatments can have an excellent performance in this application as well as in wound healing and dressing, bioadhesives, tissue engineering, and other biomedical applications.

1. Introduction

In humans, the skin is the largest organ of the body, composed of several cell layers. It is vital because it plays a central role as the first barrier against injuries and pathogens. Because of its large size, it is very susceptible to wounds, burns, trauma and microbial infections [1, 2, 3]. Damaged or compromised tissue is prone to colonization by microorganisms or pathogens such as *Staphylococcus aureus* (gram-positive bacteria) and *Escherichia coli* (gram-negative bacteria), which upon wound colonization can even form biofilms or cell aggregates [4, 5]. This can occur either by hospital infection or community transmission, which causes inflammation, deterioration of the wound and sometimes cannot be counteracted autonomously by the host organism due to the increasing antibiotic resistance developed by certain strains [2]. Moreover, microbial biofilms present low antibiotic penetration, making it even more challenging to control bacterial growth [6, 7, 8].

Indiscriminate use and self-prescription of traditional antibiotics have led to the emergence of numerous resistant microbial strains responsible for the death of nearly 35.000 people each year in the U.S. [9]. This has spurred the development of several strategies, including synthesizing highly active nanostructured materials and preparing antimicrobial micro and nanobioconjugates by interfacing nanostructured materials with antimicrobial agents such as proteins and peptides [10]. In this regard, antimicrobial peptides such as Buforin II (BUF-II), LL 37, and

* Corresponding author.
** Corresponding author.
E-mail addresses: jc.cruz@uniandes.edu.co (J.C. Cruz), lh.reyes@uniandes.edu.co (L.H. Reyes).

https://doi.org/10.1016/j.heliyon.2022.e09145
Received 9 October 2021; Received in revised form 23 November 2021; Accepted 14 March 2022

Aurein 1.2 have attracted significant attention due to stability, antimicrobial activity, low cost, and the possibility of recombinant production [11, 12, 13, 14, 15]. The potency of microparticles and nanostructured materials stands out mainly due to their area-volume ratio, size, and capacity to interact with the microbial cell membrane, allowing their applications in the pharmaceutical, cosmetics, food, and medical devices industries [16]. Some of the most popular microparticulate materials include microcapsules, microspheres, and microencapsulation on biopolymeric hydrogels.

In contrast, in the case of nanostructured ones, the preferred choices are metallic (e.g., zinc oxide, copper oxide, iron oxide, silver and gold NPs), polymeric nanoparticles (e.g., liposomes, micelles, and dendrimers), and carbonaceous nanomaterials (e.g., graphene, graphene oxide, carbon nanotubes, and carbon dots) [16, 17]. For instance, these nanostructured, microstructured, and polymeric materials have a wide variety of engineering applications, including absorbing electromagnetic waves in high frequency (GHz) requiring thin thickness, lightweight, and thermal stability [18]; coating nanomaterials with enhanced magnetic, optical, electrochemical and mechanical properties to avoid erosion and corrosion [19, 20]; nanomaterials that could arrest the problems that affect the efficiency of Li-ion batteries and, improve the storage and delivering capacity for long term cyclability [21]; and develop potential anode materials for sodium-ion batteries [22]. Moreover, there are other exciting materials such as complex iron oxides, dielectric oxides, and superconducting oxides. For instance, manganese metallic nanoparticles and spinel-type DyY co-substituted Mn–Zn nano-spinel ferrites have been successfully evaluated with anti-cancer potential in human colorectal carcinoma cells and human embryonic kidney cells; and promising antibacterial activity against *E. coli* and *S. aureus* [23, 24]. A study by Azam Ansar et al. had a similar approach with a mesoporous material with titanium dioxide (TiO_2) nanofibers. This nanomaterial was evaluated against *S. aureus* and Gram-negative *Pseudomonas aeruginosa* and exhibited an excellent ability to prevent bacterial growth and biofilm formation [25].

One of the most attractive and widely studied nanostructured materials with antimicrobial activity on its own is silver nanoparticles (Ag NPs), which also offer high chemical stability, high surface-to-volume ratio, relatively low synthesis cost, ease of preparation, and high reactivity [26, 27]. Ag NPs' antibacterial activity has been attributed to their attachment to bacterial membranes, inducing disruption, leakage of bacterial inner components, and even inhibition of protein synthesis [13]. Despite these advantages, silver nanoparticles tend to agglomerate easily due to the high surface energy and lose their catalytic efficiency and chemical stability over time [28]. As a result, several strategies have been considered, including core-shell composites and immobilization on different supports or substrates, enhancing heterogeneity, available active sites for interaction, and selectivity [29, 30, 31, 32]. Some of the most successful supports include silica, quantum dots, fluorescent chemosensors, covalent organic microspheres, reduced graphene oxide, imine-functionalized graphene oxide, and graphene oxide (GO) [31, 33, 34, 35].

Recent reports have revealed that GO offers a large surface area, low cytotoxicity, and high solubility in aqueous media, which are all needed to develop relevant applications in the biomedical field [27]. Moreover, GO is prominent support for dispersing and stabilizing Ag NPs. It combines a large specific surface area and oxygenated functionalities, acting as the anchoring sites for attaching silver nanoparticles [36]. Furthermore, GO-Ag NPs nanoplatforms exhibit enhanced antimicrobial activity compared with bare Ag NPs and show superior biocompatibility, thermal, mechanical, and optical properties, suitable for applications in photothermal therapy (PTT) in cancer treatment or a biosensor as a diagnostic device [37, 38, 39]. For these reasons, it is a suitable selection to combine these nanomaterials to include them in our topical formulation.

Formulations based on nanoparticles, hydrogels, emulsions, creams, and patches, and their combinations have been extensively explored for topical treatments [5, 40]. Among many others, natural polymers such as chitosan, poly (lactic-co-glycolic acid), guar gum, and alginate have been successfully implemented to formulate topical vehicles with dispersed active nanomaterials. This is also the case of synthetic polymers such as polyethylene glycol (PEG), polyvinyl alcohol (PVA), and polyacrylic acid (PAA) [5]. Generally, these polymers are predominantly hydrophilic and can generate porous three-dimensional matrices where an aqueous environment allows the loading of antimicrobial molecules and antibiotics and their subsequent release when in contact with body tissues. Moreover, they provide a moisturized and cool interface that has proven helpful for wound healing without sacrificing fluid and exudate absorbance while maintaining the physiological function of the skin [3, 4, 41, 42, 43, 44]. Hydrogels have been, therefore, successfully loaded with drugs and antibiotics such as diclofenac, salicylic acid, dexamethasone, and gentamicin [2, 45, 46].

PVA stands out as one of the most versatile synthetic polymers for hydrogel synthesis. It is also a promising cutaneous dressing for wound healing due to its high biocompatibility and biodegradability [47]. As active antimicrobial agents, Ag NPs have been dispersed in PVA hydrogels. Further improvement of tissue regeneration and wound recovery abilities have been achieved by mixing it or crosslinking it with polymers such as gelatin and hyaluronic acid, which have been thought to mimic the microenvironment of native tissues [48]. Gelatin is an animal protein obtained by hydrolysis of fibrous insoluble collagen that has been used in the synthesis of hydrogels, capsules, and microspheres for different biomedical applications, including drug delivery systems, wound dressings, and regenerative scaffolds. This is because gelatin has proven helpful in exudate absorption and in providing a moist environment that accelerates wound healing by promoting cell adhesion, differentiation, and proliferation mainly due to the presence of arginine-glycine-aspartate (RGD) active motif domains sequences [49, 50]. Hyaluronic acid is a linear polysaccharide found in the extracellular matrix of connective tissues. Additionally, it has viscoelastic, biocompatibility, biodegradability properties, and the capacity to retain a high amount of water. This makes it unique for promoting healing [51] and helping induce relevant cell signaling for tissue regeneration [52]. The hydrogel's mechanical properties and physical stability are typically assured by chemical or physical crosslinking [47]. Finally, another polymer that has been often incorporated into topical and cosmetic formulations is PAA, which is commercially known as Carbopol®. This polymer is also very biocompatible, has been well accepted by patients, and shows compatibility with the most active ingredients [53].

This work seeks to formulate topical antibacterial treatments based on a mixture of gelatin and PVA with dispersed GO-Ag NPs nanoconjugates as active agents. To determine whether the obtained attributes were sufficient for the final application, the prepared nanocomposites were characterized physicochemically, mechanically, microstructurally, thermally, and rheologically. Also, the routes for exfoliating the GO-Ag NPs nanoconjugates properly into the hydrogels were studied. Moreover, their biocompatibility was estimated through cytotoxicity, hemolysis, and platelet aggregation assays. Finally, antimicrobial assays against *E. coli* and *S. aureus* were conducted.

2. Materials and methods

2.1. Preparation of graphene Oxide-Ag nanoparticles conjugates

GO was synthesized according to our previous work and illustrated in Figure S 1 [54]. Briefly, 90 mL of sulfuric acid (95%) and 10 mL of phosphoric acid were mixed and added slowly to 0.75 g of graphite powder and 4.5 g of potassium permanganate. The resulting solution was left to react at 50 °C under constant magnetic stirring for 12 h. Next, 150 mL of type I water ice cubes were added to stop the oxidation. Then, hydrogen peroxide was added dropwise until a visual change was observed (from dark purple to yellow). Next, the solution was filtered with polyester fiber and centrifuged (Thermo Electron Corporation, TEC

CL40R, Waltham, Massachusetts, USA) at 4000 RPM for 4 h, supernatants were discarded, and pellets were resuspended on a washing solution of HCl 37%, ultra-pure ethanol, and type I water (1:1:1). This washing process was completed in triplicate. GO was washed twice with ultra-pure ethanol and type I water (1:1) and once with type I water. Finally, GO was stored at 4 °C until further use.

Then, silver nanoparticles were grown on the GO surface via a silver ion reduction reaction based on the work by Philip et al. with some modifications [55]. Briefly, a precursor solution of GO was prepared at 1.0 mg/mL and 0.01 *M silver* nitrate ($AgNO_3$), sonicated in an ultrasonic bath (Branson, 2510 CXP, Brookfield, Connecticut, United States) for 5 min, and left under magnetic stirring for another 10 min. In parallel, a solution of 20 g of pure bee honey, which acts as a reducing agent, was prepared in 80 mL of type II water. 75 mL of the honey solution were added for each 100 mL of the precursor solution. This mixture was sonicated for 5 min and left under magnetic stirring for ten more minutes. Then, the reduction reaction and growth of silver nanoparticles on the surface of GO was initiated. For this, the pH was adjusted to 8.5 quickly with 5M NaOH, where a color change from black to dark brown was observed, indicating the silver nanoparticles' formation. The as-synthesized material was left under magnetic agitation for 30 min and subsequently centrifuged (Thermo Electron Corporation, TEC CL40R, Waltham, Massachusetts, USA) at 4000 RPM for 4 h to concentrate it. This washing step was repeated five times with type II water. The final solution was stored at 4 °C until further use. This process is illustrated in Figure S 1.

2.1.1. Characterization of graphene Oxide-Ag nanoparticles

Graphene oxide and Graphene Oxide-Ag Nanoparticles were characterized via FTIR, TGA, UV-Vis, Z-potential, Raman spectroscopy, XRD, SEM-EDX, and TEM analysis. Fourier transform infrared spectroscopy spectra were recorded in a Bruker Alpha II (Bruker, Germany) in a range of 4000–600 cm^{-1} with a spectral resolution of 2 cm^{-1}. Thermogravimetric analysis was performed in a Q600 Simultaneous TGA/DSC (TA Instruments, New Castle, DE, USA) for a temperature range from 25 to 600 °C and a heating rate of 10 °C/min under a Nitrogen atmosphere (gas flow: 100 mL/min). UV-Vis spectra were recorded using a UV-Vis spectrophotometer (Mettler Toledo V 670, United States) in a range of 300–700 nm. Raman spectra were recorded in the range of 100–3000 cm^{-1} with a laser of 532 nm and an objective 100x/0.75 NIR using an XPlora Raman Horiba confocal (Horiba Scientific, Japan). XRD spectra were recorded using a Malvern-Panalytical-Empyrean model (45kV, 40mA) (Malvern Panalytical, United Kingdom) in the range of 5°–80°. SEM-EDX analyses were carried out in an FE-MEB LYRA3 (Tescan, Czech Republic) attached with an energy-dispersive X-ray spectroscopy system for elemental analysis. Transmission electron microscopy (TEM) images were collected on a Tecnai F30 TEM (FEI Company, Fremont, CA, USA).

2.2. Preparation of gelatin/polyvinyl-alcohol hydrogels

Sterile milli-Q water was heated up to 50 °C and 80 °C in a hot plate and mixed with gelatin Type A (food grade) and polyvinyl-alcohol (PVA) (Mw 89,000–98,000, 99+% hydrolyzed, Sigma Aldrich, Germany), respectively. Then, each polymer solution was sterilized by syringe filtration with a 0.22 μm filter (Sartorius, Minisart, Göttingen, Germany). The mixture was degassed for 5 min in an ultrasonic bath (Branson, 2510 CXP, Brookfield, Connecticut, United States). The mixture was kept at 50 °C under constant stirring with a mechanical agitator (Heidolph, Schwabach, Germany) at 250 RPM while slowly adding hyaluronic acid and triethanolamine. The GO-Ag NPs nanoconjugates (if needed) were added for about 7 min until a homogeneous mixture was formed. For hydrogels in the absence of the nanoconjugates, Carbopol 940® was added, and stirring continued at 500 RPM for 30 more minutes. In the case of hydrogels in the presence of nanoconjugates, stirring at 1000 RPM continued for 45 more minutes [56]. Finally, the obtained hydrogels were stored at room temperature in closed glass containers until further use. The entire procedure was completed using sterilized materials and equipment in a laminar flow cabinet.

Table 1. Experimental design used to study the influence of the concentration of gelatin and polyvinyl alcohol in hydrogels as a topical antimicrobial treatment.

Sample	Gelatin (% w/v)	PVA (% w/v)	Carbopol (% w/v)	Triethanolamine (w/v)	Hyaluronic acid (% v/v)
1	0.7	0.1	0.2	0.2	0.5
2	0.7	0.4			
3	0.7	0.7			
4	1.1	0.1			
5	1.1	0.4			
6	1.1	0.7			
7	1.5	0.1			
8	1.5	0.4			
9	1.5	0.7			

2.3. Experimental design

For characterization purposes, a 3^2 experimental design (2 factors with three levels each one) was used. The factors evaluated were the concentrations of gelatin and PVA in the hydrogel. The three gelatin concentrations selected for this study were 0.7%, 1.1% and 1.5% (w/v) while those of PVA were 0.1%, 0.4% and 0.7% (w/v). The triethanolamine and hyaluronic acid concentrations were kept at the same level for all treatments. The selected concentrations were also previously reported for other hydrogels [42, 57, 58, 59]. The nanoconjugate encapsulation proceeded according to the results of the thermal, mechanical, rheological, morphological, particle size, and stability characterization of the hydrogels (see below for details). The experimental design followed is presented in Table 1. The best performing formulations were selected for nanoconjugate encapsulation. For such analyses, the experimental design is shown in Table 2. Additionally, commercially available topical treatments in Colombia were included in the experimental design as controls. The selected products were Zudenina Plus Gel® (Medihealth, Colombia) and Microdacyn Top Hydrogel® (More Pharma Corporation, Mexico). All the characterizations were applied to both the prepared hydrogels and the commercial products.

2.4. Microscopic characterization of topical formulations

The structure and morphology of the prepared hydrogels were imaged with a JEOL scanning electron microscope (model JSM 6490-LV). The observation was performed directly on a cooling stage at −15 °C with a liquid nitrogen-mediated fracturing setup to avoid alterations of the gel structure. Twelve high-resolution images per treatment were obtained at 1500X and 3000X magnifications (10 kV). These images were analyzed further to determine the average pore size of each hydrogel aided by the software ImageJ® [61]. This software develops a mask for identifying pores with sphericity between 0.4 and 0.9 and a table of results where possible pores or wrongly identified values can be discarded. Additionally, hydrogels with dispersed nanoconjugates were observed to investigate possible changes in their microstructure and, consequently, in pore size.

2.5. Thermal stability analyses

Thermogravimetric analyses (TGA) were conducted in the range of 20–650 °C to estimate the thermal stability of the hydrogels when they were heated up at a constant rate (10 °C/min). TGA was carried out for a sample of about 15–20 mg under a controlled inert atmosphere by a supply of 100 mL/min ultra-high purity (UHP) Nitrogen. The instrument

Table 2. Experimental design used to study the influence of the concentration of gelatin in hydrogels on the encapsulation of GO-Ag NP nanoconjugate as a topical antimicrobial treatment.

Sample	Gelatin (% w/v)	PVA (% w/v)	Carbopol (% w/v)	Triethanolamine (w/v)	Hyaluronic acid (% v/v)	GO-Ag NP nanoconjugate (μg/mL) [60]
1	1.1	0.7	0.2	0.2	0.5	20
2	1.5	0.7				

used for the tests was the Q600 Simultaneous TGA/DSC (TA Instruments, New Castle, DE, USA).

2.6. Rheological response

The rheological analyses were carried out in a Discovery Series Hybrid Rheometer-1 (TA Instruments, New Castle, DE, USA) by running an oscillatory frequency scan between 0.62 and 62 rad/s, or its equivalent between 1 and 10 Hz [62], at a constant amplitude of 100 Pa and 20 °C. A flow sweep was evaluated between 0.1 and 200 1/s and 20 °C. A parallel plate (diameter 20 mm) geometry was used with a fixed gap distance (1.0 mm) between the plates. A sample amount corresponding to 20 mm diameter and 1 mm thickness was used for this characterization (200–300 mg). The power law (Eq. 1.) was used to calculate the flow index and to know the behavior of the fluid [54, 63, 64].

$$\tau = k\,\gamma^{\eta} \tag{1}$$

Where τ is the shear stress, γ is the shear rate, k is the consistency index, and η is the flow index.

2.7. Textural properties analysis

The traditional texture profile analysis (TPA) was evaluated with the aid of a TA.HDplusC Texture Analyzer (Stable Micro Systems, Godalming, United Kingdom). The tests measured hardness, compressibility, adhesiveness, and cohesiveness through a double compression cycle at 5 mm/s with a 35 mm cylindrical probe and 20 mm depth penetration [64]. Measurements were conducted for hydrogels in glass containers by maintaining the same fluid height at room temperature for all treatments.

2.8. Hydrogel particle size evaluation

The particle size distribution of each hydrogel sample was evaluated with a static light scattering (SLS) technique on the Hydro MV unite in Mastersizer 3000 (Malvern Panalytical, Malvern, Worcestershire, England). The volume-weighted average diameter (d_{43}) was regarded as the mean diameter for all measurements. Gelatin was used as reference material, and the obscuration was set between 5 and 15% using water as a dispersant at 1300 RPM constant agitation [65, 66, 67].

2.9. Hydrogel stability

Two routes were assessed for interrogating the stability of topical treatments. The first one was the physical stability by monitoring in the Turbiscan LAB instrument (Formulaction Smart scientific analysis, Toulouse, France) through Multiple Light Scattering – MLS technology. The second one was by tracking the aging of the treatment under a controlled environment in the RGX-250E stability and growth chamber (Thomson, Ningbo, China).

2.9.1. Physical stability

The stability of the treatment was measured by the Turbiscan stability index (TSI) over one month of aging in the stability chamber. The sample was transferred to borosilicated cylindrical glass vials without any dilution and scanned from bottom to top at 25 °C. A 25 s scan was performed periodically (every 2–3 days) for a month [68].

2.9.2. Aging under controlled conditions

The treatment was based on the "Guide for the development and submission of stability studies of chemically synthesized drugs" of the Ministry of Health and Social Protection of Colombia [69]. This was performed for the short-term under accelerated stability conditions at 40 °C and 75% relative humidity (RH) for one month [70]. Particle size analysis, TPA, and rheological behavior were measured at 7, 14, and 28 days of aging in the stability chamber compared with a freshly prepared hydrogel sample.

2.10. Hemolysis assay

A hemolysis activity assay was conducted to evaluate the hemocompatibility of the topical hydrogels' formulations. This assay was performed following the guidelines of ISO 10993-4 with slight modifications [71]. Briefly, blood was withdrawn from a healthy human donor and transferred to EDTA tubes. The samples were obtained with the approval of the Ethical Committee at the Universidad de los Andes (minute number 928–2018). The sample was centrifuged (Thermo Electron Corporation, TEC CL40R, Waltham, Massachusetts, USA) at 1800 RPM for 5 min. The supernatant was discarded, and the sample was then washed with 150 mM NaCl solution and centrifuged again. This procedure was performed in triplicate. The supernatant was checked for low turbidity and discarded. PBS 1X at pH 7.4 was added to gently resuspend the erythrocytes. A 1:10 dilution of a concentrated solution of erythrocytes in PBS 1X was performed to obtain $\sim 3 \times 10^7$ erythrocytes/mL according to a Neubauer chamber count. Previously, flat-bottomed 96-well microtiter plates were prepared with 100 μL of PBS per well, where serial dilutions of the formulated and commercial topicals were formed. PBS 1X was used as the negative control and Triton X-100 as the positive control. 100 μL of erythrocyte suspension was then transferred to the well. The microplates were incubated at 37 °C for 1 h and subsequently centrifuged (Thermo Electron Corporation, TEC CL40R, Waltham, Massachusetts, USA) at 1260 RPM for 5 min at room temperature. The supernatant was carefully removed and placed in another microplate to read the absorbance at 450 nm in the microplate absorbance spectrophotometer (Thermo Scientific, Waltham, Massachusetts, United States) [72].

2.11. Platelet aggregation assay

Blood was withdrawn from a healthy human donor and transferred to sodium citrate tubes. The samples were obtained with the approval of the Ethical Committee at the Universidad de los Andes (minute number 928–2018). The sample was centrifuged (Thermo Electron Corporation, TEC CL40R, Waltham, Massachusetts, USA) at 1000 RPM for 15 min to obtain platelet-rich plasma (PRP). Previously, flat-bottomed 96-well microtiter plates were prepared with 70 μL of PBS per well, where serial dilutions of the formulated and commercial treatments were formed. Platelet-poor plasma was used as the negative control and Thrombin (6U) as the positive control. 30 μL of PRP solution was then added to each well. The microplates were incubated at room temperature for 3 min. Next, the absorbance was read at 620 nm in a microplate spectrophotometer (Thermo Scientific, Waltham, Massachusetts, United States) [73].

2.12. Antimicrobial activity determination

This assay was based on "*Performance Standards for Antimicrobial Disk Susceptibility Tests*" from the Clinical and Laboratory Standards Institute

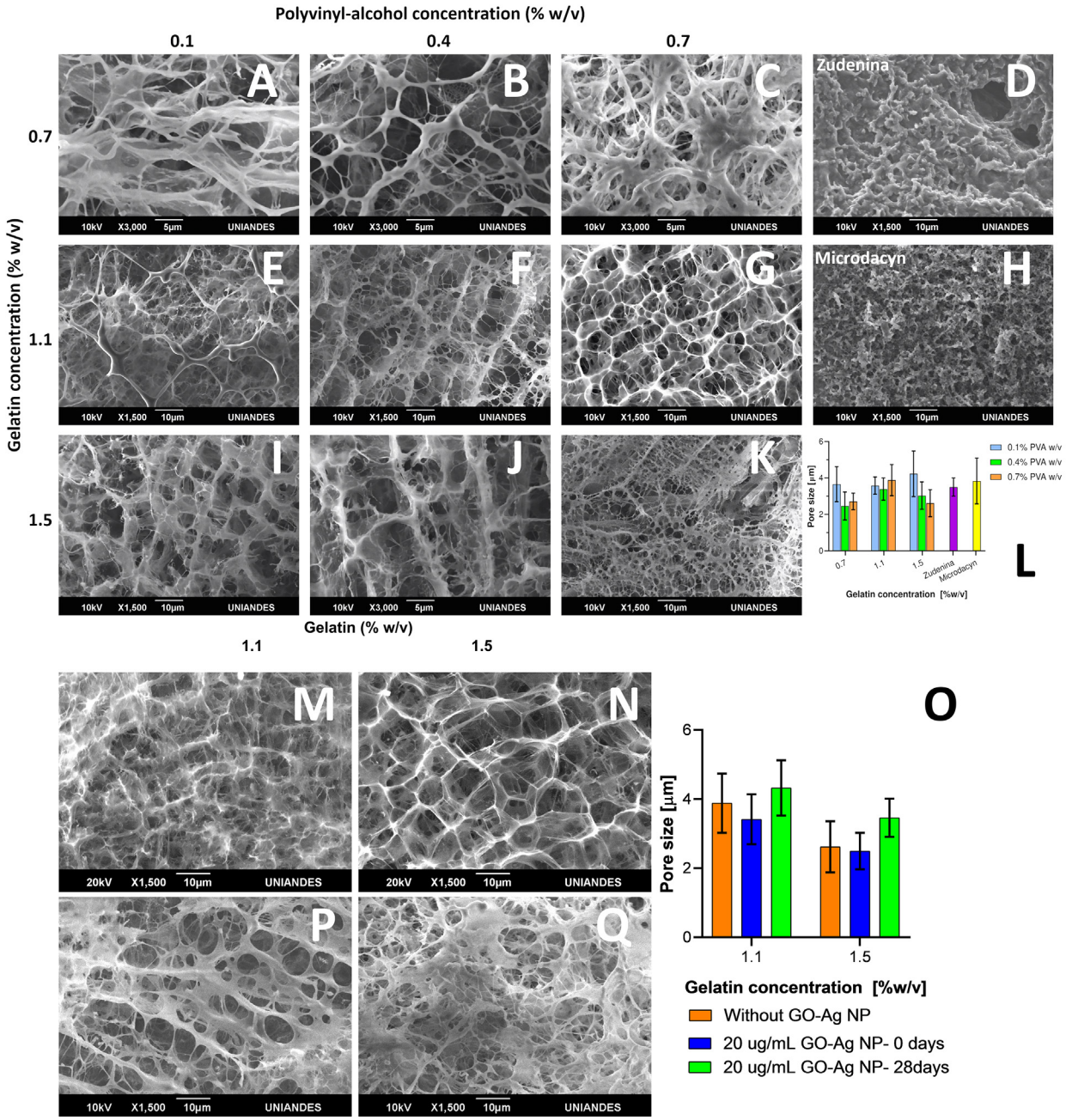

Figure 1. Surface morphology described by scanning electron microscope (SEM) micrographs of cross-linked hydrogels in the presence and absence of GO-Ag NPs. First row is for 0.7% (w/v) gelatin concentration and varying PVA concentrations from 0.1% (**A**), 0.4% (**B**) to 0.7% (w/v) (**C**). Additionally, the Zudenina® micrograph is presented (**D**). Second row is for 1.1% (w/v) gelatin concentration and varying PVA concentrations 0.1% (**E**), 0.4% (**F**) to 0.7% (w/v) (**G**). Additionally, the Microdacyn® micrograph is presented (**H**). Finally, 1.5% (w/v) gelatin concentration and varying PVA concentrations from 0.1% (**I**), 0.4% (**J**) to 0.7% (w/v) (**K**). Average pore size for all treatments is shown (**L**). 0.7% (w/v) PVA, 20 µg/mL GO-Ag NPs, 1.1% (**M**) and 1.5% (**N**) (w/w) gelatin hydrogel are presented at 0 days and at 28 days aging (**P**) and (**Q**) respectively with average pore size (**O**).

with slight modifications [74]. Wild-type bacterial strains of *E. coli* and *S. aureus* were used for this assay. 10 µL of cryostat culture were seeded on Lysogeny broth (LB) agar (casein peptone 1.0% w/v, yeast extract 0.5% w/v, sodium chloride 0.5% w/v, agar 2.0% w/v) plates. These were then incubated for 16 h at 37 °C. One isolated colony was selected and inoculated in 5 mL of liquid LB in 15 mL Falcon tubes followed by incubation at 37 °C and 250 RPM for 3 h. This culture was centrifuged (Thermo Electron Corporation, TEC CL40R, Waltham, Massachusetts, USA) at 3000 RPM and 4 °C for 5 min. The supernatant was discarded, and 2 mL of 9.45 mM disodium phosphate (Na_2HPO_4) buffer solution at pH 7.4 was added and resuspended. This procedure was repeated twice, and at the end of the washing process, the absorbance of the culture was recorded at 595 nm in a microplate spectrophotometer (Thermo Scientific, Waltham, Massachusetts, United States). This was used to determine the concentration (CFU/mL) aided by a previous calibration curve for the growth of each bacterial culture. A dilution in buffer solution was performed to obtain a culture with 1×10^7 CFU/mL. In parallel, 500 µL of each formulation and the commercial topical treatment was added to 2 mL Eppendorf tubes, to which 500 µL of bacterial culture was then pipetted. Only bacterial culture was considered the positive control, and

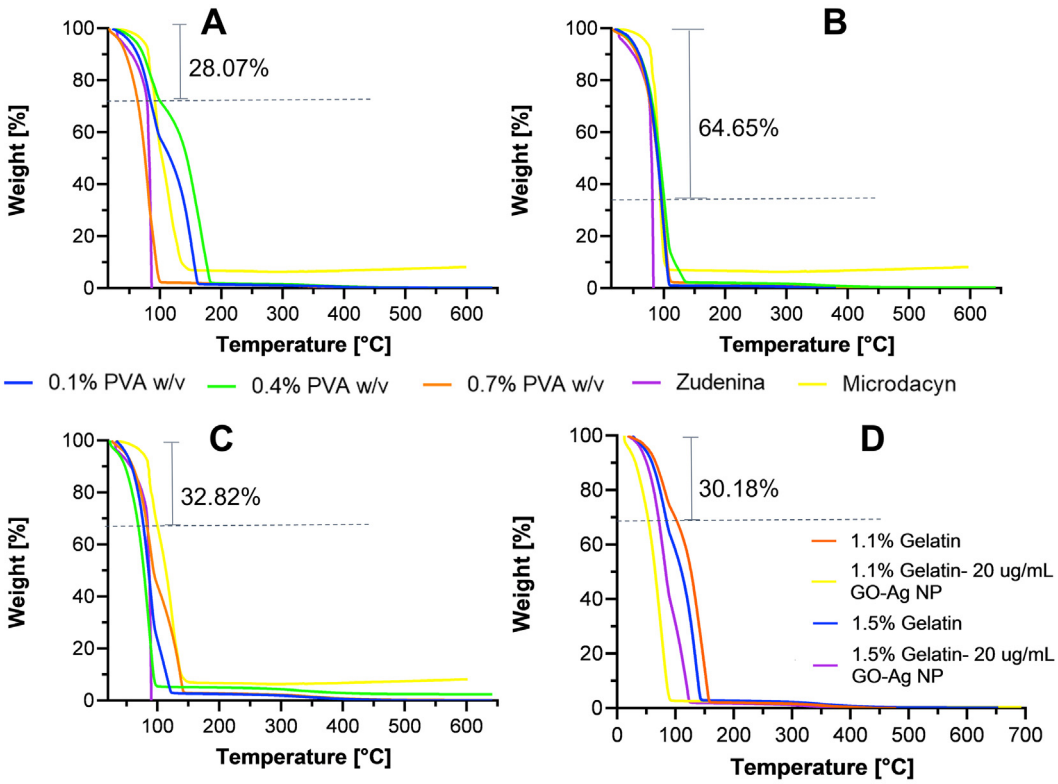

Figure 2. The minimum weight (%) loss at 100 °C is indicated in each plot. Thermograms for hydrogels with 0.7% (**A**), 1.1% (**B**) and 1.5% (**C**) (w/v) gelatin concentration. PVA concentrations of 0.1% (w/v) (blue), 0.4% (w/v) (green), and 0.7% (w/v) (orange). Also, Zudenina® (purple) and Microdacyn® (yellow) are shown. Thermal degradation after GO-Ag NPs incorporation for hydrogels with 1.1% and 1.5% (**D**) (w/v) gelatin concentration.

the medium was the negative one. These experiments were conducted in triplicate at 37 °C for 2 h. At the end of incubation, they were resuspended, and the next 10^{-5} serial dilutions were carried out starting with 100 μL. The last dilution tube was seeded in Mueller-Hinton agar (3.7% (w/v)) plates with sterile swabs and incubated at 37 °C for 18 h. Finally, the colonies per plate were counted to calculate the percentage of bacterial growth [75].

2.13. Evaluation of cell viability via MTT assay

Cytotoxicity of 1.1% and 1.5 % Gelatin-20ug/mL GO-Ag NPs hydrogels was evaluated by quantifying the metabolic activity of Vero cells (ATCC® CCL-81) via MTT assay. Briefly, cells suspended in supplemented DMEM medium (10% FBS) were seeded on 96-well microplates at a cellular density of 10^4 cells/well and then incubated at 37 °C, 5% CO_2 for 24 h. Next, supplemented DMEM medium was replaced by the non-supplemented DMEM medium extracts of the different hydrogels at serial dilutions from 50 to 1.56 % (v/v). The extracts of the hydrogels were made according to the guideline of the international standard ISO 10993-5:2009. Cells were then incubated at the same conditions for 24 and 48 h. After the incubation time, 10 μL of MTT solution (5 mg/mL) were added to each well, and the microplates were incubated for 2 h. Finally, supernatants were carefully discarded, and DMSO (100 μL/well) was added to dissolve formazan crystals. Absorbance was read at 595 nm in a microplate reader, and cell viability was finally calculated by following the equation: Cell viability (%) = Abs (sample) * 100/Abs (negative control).

2.14. Statistical analysis

In all experiments, a Q test was performed to discard outliers, and then the statistical analysis of the results was performed by analysis of variance (ANOVA), with a p-value <0.05 considered as statistically significant. Also, a student's t-test was conducted to determine significant differences between treatment means. The statistical analyses were performed in the software Minitab®.

3. Results and discussion

3.1. Morphological structure

The collected SEM micrographs shown in Figure 1 A-K present an interconnected 3D polymeric network for all hydrogel topical treatments without observable signs of phase separation [76]. This is because of the physical crosslinking between the polymeric chains of gelatin, PVA and Carbopol®. A strong mesh interaction is observed, becoming more evident and cross-linked as the amount of gelatin and PVA included in the formulation increases [77]. Similarly, in hydrogels with lower polymer concentration, occluded water predominates, so the pores will tend to be more prominent [78]. After dispersing the nanoconjugate in the topical hydrogel treatment formulation, the microstructure and its mean pore size are shown in Figure 1 M-O. As shown in Figure 1 L and Figure 1 O, no observable and statistically significant differences in the microstructure were found as reported in previous studies [76]. No GO-Ag NPs aggregates were identified, which was not expected due to the resolution of the imaging instrument. This allowed us to conclude that their dispersion within the polymeric matrix was successful without significant changes in the structural conformation of the 3D matrix. The average pore size analysis performed in Figure 1 L shows no significant difference between treatments. Still, they show a tendency to pore reduction as PVA concentration increases or when gelatin increases (Figure 1 O). This is favorable for the application of this study, which requires encapsulation of GO-Ag NPs nanoconjugates within pores [79, 80]. Figure 1 D and H show the microstructure of commercial treatments, which are much less porous and organized than our formulations. This is most likely due to aggregates of dispersed active compounds and water.

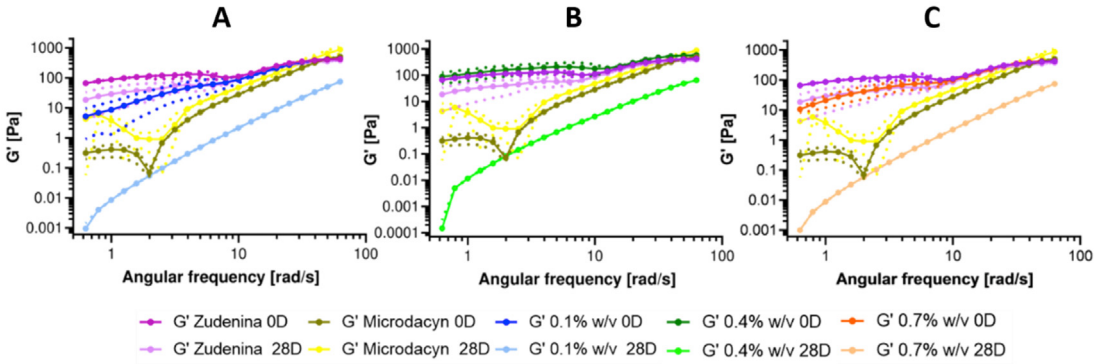

Figure 3. Storage modulus for hydrogels at 0.7% (w/v) gelatin, 0.1% (**A**), 0.4% (**B**), 0.7% (**C**) (w/v) freshly prepared PVA after 28 days of accelerated aging conditions at 40 °C and 75% RH. Commercial treatments Zudenina® and Microdacyn® are also included for comparison.

Micrographs collected after 28 days of aging (see Figure 1 P-Q) show that the pore size of the topical treatments increased slightly, which may be related to the mobility of polymeric chains, and the molecular destabilization due to heat and humidity under accelerated stability conditions.

The study of the microstructure of the topical treatment showed compact and evident crosslinking between the incorporated polymers. For the evaluated gelatin, PVA, and the nanoconjugate amounts, no apparent alteration of the microstructural conformation of the hydrogel was observed, contrary to what Khorasani et al. described for high nanoparticles concentrations [81]. It was also concluded that these micropores or microchambers are suitable for releasing our active compound when applied to the infected skin area [82].

3.2. Thermal resistance evaluation and characterization of GO-Ag NPs

Thermogravimetric analyses were conducted in the range of room temperature to 650 °C to estimate the nanocomposite hydrogels' thermal stability before and after GO-Ag NPs dispersion in the formulations. As observed in our previous work [54, 83], Figure 2 shows an initial noticeable weight loss at 100 °C that varies from approximately 28%–65% depending on the formulation. This can be directly related to the evaporation of the water occluded within the hydrogel. However, it is remarkable that the polymeric material can retain and adsorb water in its interior due to the crosslinking of the polymer network, which is a critical feature for wound skin healing [77, 84, 85]. In general terms, no clear trend is observed in the thermal resistance of the prepared topical treatments. The presence of PVA leads to no impact on the thermal stability of the formulations. For the cases of 0.7% and 1.1% (w/v) gelatin (Figure 2 A and B), the polymeric structure is stable up to 250 °C, where decarboxylation is likely present, as has been reported previously [86]. At that point, the 1.5% (w/v) gelatin formulation (Figure 2 C) shows a subtle improvement, evidenced by 6%–9% remaining weight up to 350 °C. This indicates a much more stable structure, followed by decomposition into carbonaceous residues, and finally, the complete disintegration of the network [87].

The commercial topical treatment Zudenina® is highly thermally unstable, evidenced by almost a complete degradation at 100 °C. On the contrary, Microdacyn® showed superior performance, retaining about 8% of its weight up to 650 °C. When the same study was carried out for topical treatments with the nanoconjugate already included, a decrease in thermal resistance was observed with respect to the pristine material. The main difference primarily occurs between 100-150 °C, where oxygen-containing functional groups from GO are degraded [88]. This is consistent with the thermal stability evaluation of the GO-AgNPs nanoconjugate, which can be seen in Figure S 2. As a result, an even more pronounced drop in weight was observed by dispersing a material that is not very thermally resistant such as the GO-AgNPs nanoconjugate in the hydrogels. This behavior agrees well with previous studies [89].

3.2.1. Characterization of GO-Ag NPs

Figure S 2 shows the different characterization techniques implemented to confirm the correct synthesis of GO and GO-Ag NPs. **Figure S 2** A shows the Raman spectra for GO and GO-Ag NPs. The characteristic peaks at 1320 and 1570 cm^{-1} corresponding to the D and G bands are identified. A ratio ID/IG higher than 1 in both spectra confirms the presence of hydroxyl and epoxide groups and the presence of Ag NPs that increases the GO's degree of disorder [90]. **Figure S 2** B shows the FTIR spectra of GO and GO-Ag NPs. FTIR spectra of both materials show several peaks, in particular, peaks at 3240 cm^{-1} related to OH groups, 1684 cm^{-1} that corresponds to stretching vibrations of C=O carboxylic moieties, 1621 cm^{-1} to aromatic C=C bond vibrations, as well as peaks at 1365 cm^{-1}, 1215 $cm^{-1,}$ and 1054 cm^{-1} corresponding to C–O–H deformation, C–H (epoxy) stretching and C–O (alkoxy), respectively. Moreover, the GO-Ag NPs spectrum shows an increase in the intensity of the peaks related to C=C, C–H, and C–O, confirming the interaction between Ag NPs and the oxygen-containing functional groups on the surface of GO nanosheets [90, 91]. **Figure S 2** C shows the thermograms of GO and GO-Ag NPs. In both spectra, we can observe the presence of a substantial weight loss, 43.5% for GO and 95.2% for GO-Ag NPs, related to the release of oxygen-containing functional groups. These results demonstrated poor thermal stability for both materials at temperatures above 100 °C. However, that does not pose a limitation for their applicability in the synthesis of topical treatments in which the manufacturing and application temperatures are lower than 40 °C. Z-Potential analysis showed large negative values for GO (-43.5 ± 1.5 mV) and GO-Ag NPs (39 ± 2 mV), confirming high dispersity, significant long-term stability, and no aggregation in type I water at pH = 7 [91]. **Figure S 2** D and E show the UV-Vis spectra for GO and GO-Ag NPS and the XRD patterns, respectively. UV-Vis spectrum for GO-Ag NPS exposes a critical absorbance peak at 400 nm that confirms the synthesis of Ag NPs on the surface of GO. This result is confirmed via TEM image analysis (**Figure S 2 F**), where the presence of Ag NPs of different sizes throughout the surface of the GO nanosheets is easily identifiable [91, 92]. XRD pattern of GO exposed a remarkable peak at 9.3°, which corresponds to the (001) plane, and an additional one at 29.1° associated with the (002) plane. The pattern of GO-Ag NPs showed four intense peaks at 38.4°, 46.5°, 64.7° and 77.46°, which are assigned to (111), (200), (220) and (311) planes of Ag NPs (JCPDS No. 04–0783), respectively [92]. In addition, the peak at 28.1° is associated with the (002) plane of GO with a slight shift. These results confirm the presence of the Ag NPs in the face-centered cubic phase deposited on the surface of GO [91]. Finally, the presence of Ag

Table 3. Storage modulus at 1 and 62 rad/s for 1.1 and 1.5% (w/v) gelatin concentration at 0 and 28 aging days.

Formulation		G' [Pa] at 1 rad/s		G' [Pa] at 62 rad/s	
Gelatin	**PVA**	**0 d**	**28 d**	**0 d**	**28 d**
1.1	0.1	8.67 ± 5.48	0.008 ± 0.0009	470.19 ± 11.97	73.98 ± 2.66
1.1	0.4	7.87 ± 6.67	0.043 ± 0.014	422.92 ± 31.78	44.07 ± 14.58
1.1	0.7	64.45 ± 63.63	4.46 ± 0.002	515.27 ± 160.57	164.37 ± 7.92
1.5	0.1	24.24 ± 17.15	0.045 ± 0.014	440.54 ± 52.54	36.13 ± 13.54
1.5	0.4	10.65 ± 1.72	0.026 ± 0.0003	463.67 ± 8.09	56.30 ± 10.31
1.5	0.7	40.22 ± 29.74	3.2 ± 0.0004	693.04 ± 269.04	112.30 ± 0.27

NPs on the surface of GO was also confirmed via SEM-EDX analysis (**Figure S 3**), in which the EDS spectra exposed typical peaks for C and O for GO and GO-Ag Nps and a remarkable one for Ag for GO-Ag NPs [92].

3.3. Hydrogel topical treatment rheological behavior

The oscillatory frequency test shown in Figure 3 reveals that the elastic modulus (G′) is angular frequency-dependent, indicating that the crosslinking density was insufficient to lead to a material with a complete solid-like behavior, which is a favorable attribute for a topical treatment that should spread easily and remain attached to the skin. This pseudoplastic behavior ensures that the product flows after stress application to form a thin film on the epidermis. Still, when the stress is decreased, a viscosity increase is expected to help maintain it attached to the surface [64]. G′ in all samples exhibits an increasing trend in magnitude as the angular frequency increases. This behavior is even more pronounced when the sample has completed 28 days at accelerated aging conditions. At that time and low angular frequencies, G′ varies between 1×10^{-1} and 1×10^{-3} Pa. Figure 3 shows that the hydrogels with 0.7% (w/v) gelatin and all PVA concentrations have a significant structural loss of integrity as evidenced by a decrease in G' by about four to six orders of magnitude after 28 days of aging. This is confirmed in **Figure S 4**, where it is observed that their viscosity has drastically reduced, evidencing that the pseudoplastic behavior fails to continue. This notion is also supported by the proximity of the flow index to 1 (**Figure S 6**), resembling a Newtonian fluid. These results indicate that, after one month under the accelerated aging test, the material with this level of gelatin no longer behaves like a hydrogel (in a pseudoplastic regime). This can be explained by a considerable chain rearrangement, changes in orientation or chain mobility, induced disorder at the molecular level, and unstable or insufficient cross-linking [54]. For this reason, hydrogels with this gelatin concentration were discarded as viable candidates for nanoconjugate encapsulation.

Table 3 presents the storage modulus behavior for the other freshly prepared formulations and, after the month of aging, observed at angular frequencies representing the extremes of the oscillatory sweep. There is an average loss of 99% in the G′ magnitude at 1 rad/s for the samples with 0.1 and 0.4% PVA and both gelatin concentrations. But in the instances with 0.7% PVA, the elastic modulus resistance was between 7 and 9% higher at low frequencies and between 9 and 21% at high frequencies, which helped us select these hydrogels as candidates for encapsulation. In other words, the rheological behavior performs better at high concentrations of PVA and gelatin. For hydrogels with 1.1% (w/v) gelatin, the molecular structure degradation occurs at a lower level, presenting a decrease in G′ between two and four orders of magnitude at low frequencies after 28 days under accelerated aging conditions. However, the material manages to recover as the angular frequency increases, which occurs more clearly at the higher PVA concentrations. Similar behavior was observed for the viscosity at this gelatin concentration level (**Figure S 4**). The viscosity remained more stable with increased PVA concentration, allowing to retain the typical pseudoplastic behavior of hydrogels [44]. For topicals with 1.5% (w/v) gelatin, the effect on the molecular structure is more subtle, as evidenced by the high G' and viscosity values. In this case, again, high concentrations of PVA help maintain a marked pseudoplastic behavior [79, 93]. The triethanolamine makes the matrix even more elastic [63]. Importantly, data variability was relatively low, making the material synthesis repeatable.

Interestingly, the G′ of Zudenina® shows a behavior similar to our freshly prepared topical treatments. It even presents higher stability after 28 days of aging conditions since the decrease in G' was below one order of magnitude. A similar trend was also observed for the viscosity, with no appreciable change in time. In contrast, Microdacyn® performs differently from all other samples. G′ decreases smoothly at low frequencies until it reaches a minimum of a specific frequency where the modulus increases. This is probably due to a metastable equilibrium state that changes the conformation of the base polymer and the presence of hypochlorous acid. Somewhat surprisingly, after 28 days, G′ shows a subtle increase that could be explained by the loss of moisture in the microstructure, which in turn leads to a less flexible material and, consequently, to the observed increase in G′ at low frequencies. Further

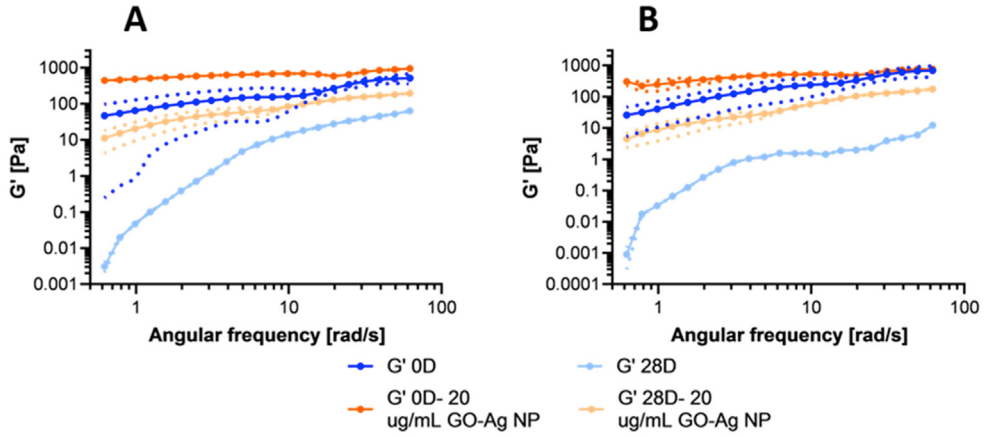

Figure 4. Storage modulus for nanocomposite hydrogels with 0.7% (w/v) PVA, 20 μg/mL GO-Ag NPs, 1.1% (w/v) gelatin (**A**), and 1.5% (w/v) gelatin (**B**), freshly prepared and after 28 days of accelerated aging conditions at 40 °C and 75% RH.

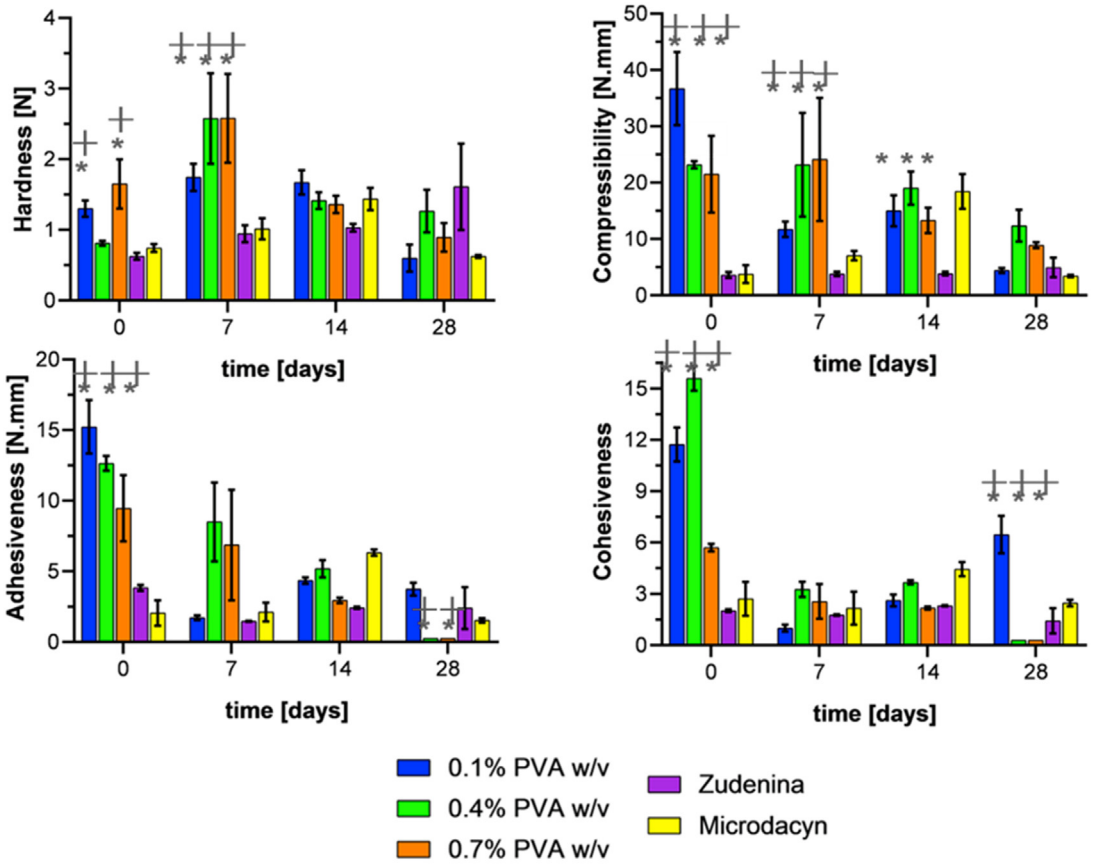

Figure 5. Texture profile analysis for freshly prepared hydrogels at 1.1% (w/v) gelatin and evaluated after 7-, 14-, and 28-days exposure to accelerated aging conditions at 40 °C and 75% RH. Commercial treatments Zudenina® and Microdacyn® are also included for comparison. *, $p < 0.05$.

evidence supporting this notion has been observed for the viscosity, where one order of magnitude increase was detected after 28 days of aging (see **Figure S 4**).

Figure 4 shows that for both formulations (1.1% and 1.5% (w/v) gelatin), the presence of the nanoconjugates led to higher G'. This behavior was observed for both freshly prepared and aged samples (after 28 days). This increase in mechanical strength and stiffness has also been reported for other hydrogel nanocomposites, e.g., carbon quantum dots, collagen, and polyacrylamide hydrogels with silver nanoparticles [2, 94, 95]. Despite this superior behavior, there is still some degradation, as evidenced by a decrease in G' after 28 days compared with the fresh samples. In line with these results, **Figure S 5** shows that the viscosity increases and is more stable in samples that contain the nanoconjugate.

G' depended not only on the angular frequency but also on the concentration of the different polymers incorporated in the formulation [64]. In contrast to the work by Park et al. [96], our results strongly suggest that by including the nanoconjugate, the polymeric network might be reinforced at the nanostructure level, thereby allowing an enhanced rheological behavior over time [89].

3.4. Texture profile analysis (TPA)

TPA experiments allowed us to estimate hardness (maximum force of the first compression), compressibility (the work required to deform the product during compression), adhesiveness (area under the zero-force line, which represents the amount of work needed to overcome attractive forces of the formulation to the compression plate), and cohesiveness (the ratio of work done on the sample during the second bite divided by the work done on the sample during the first bite) of the formulations. Hardness is related to the ease of application on the skin, while compressibility and adhesiveness with the ability to stay attached to the skin. However, the cohesiveness is related to whether the hydrogel can recover its structural stability [64, 93].

Figure 5 shows the texture profile analysis of the topical formulations with 1.1% (w/v) gelatin. The hardness of the material showed a relatively stable behavior and remained in the range of 0.5–3.5 N with no statistically significant difference after 28 days between the fresh hydrogel and the aged one. The lower hardness of the hydrogels correlates well with the uneven microstructure observed in the SEM micrographs (Figure 1) [97]. This behavior was also observed for the commercial topical treatments, which present modest hardness values, considering their mode of use and application objective. Compressibility showed significant variability among formulations. However, no clear trend was observed. What is evident is that at the end of the 28 days of aging, the compressibility was compromised for the three PVA concentrations evaluated compared with the fresh formulations. In contrast, the commercial treatments showed little variability over time, albeit at a lower level. Adhesiveness starts at values between 10-15 N.mm; however, as time passed, it consistently decreased below 5 N.mm, even reaching values close to zero for formulations with high PVA concentrations. This likely indicates a high degree of degradation and incapacity to remain attached to surfaces for relatively long periods. The commercial treatments show no marked changes in adhesiveness after 28 days of aging. In contrast, cohesiveness started with values between 6 and 15, decreased with time, and ended close to zero for formulations with high PVA concentrations. In other words, these formulations degrade under the harsh conditions of accelerated aging, which is likely due to a loss in intermolecular strength. The properties of the commercial treatments are again consistent and remain at the starting levels [93, 97, 98, 99].

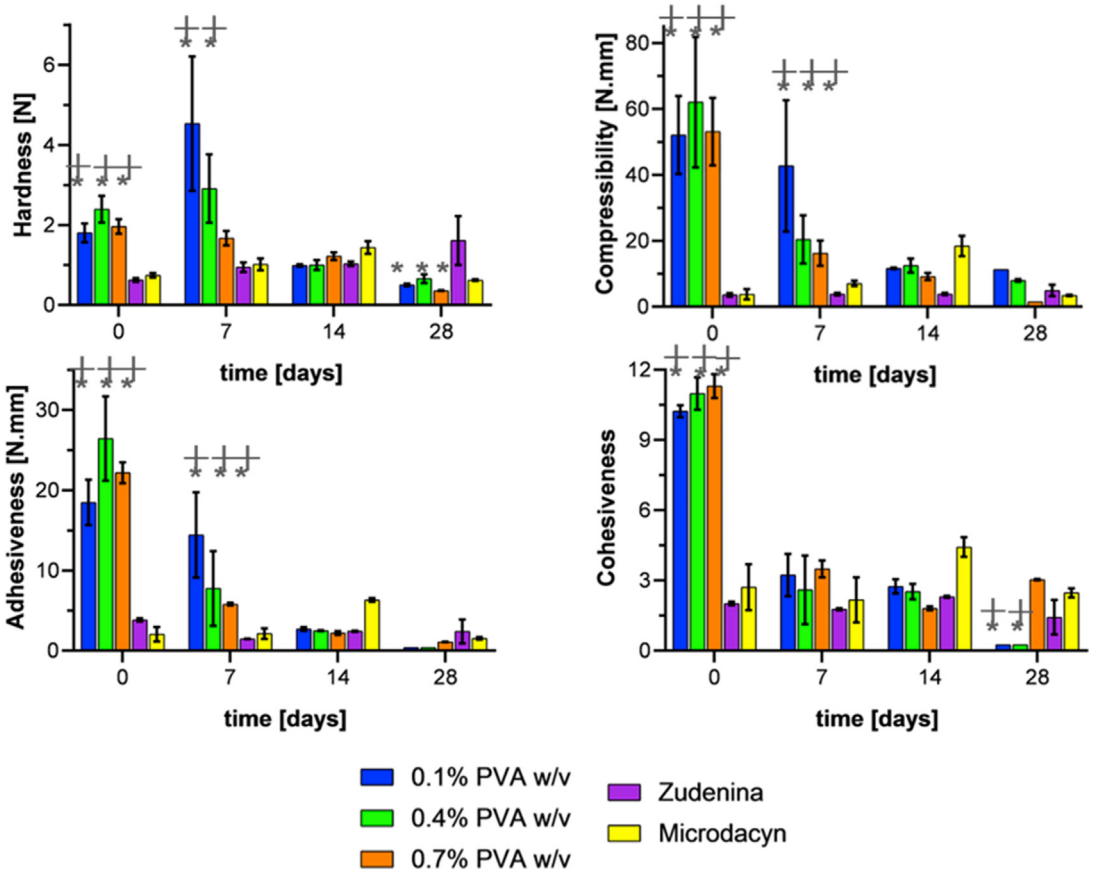

Figure 6. Texture profile analysis for hydrogels at 1.5% (w/v) gelatin freshly prepared and evaluated at 7-, 14-, and 28-days exposure to accelerated aging conditions at 40 °C and 75% RH. Commercial treatments Zudenina® and Microdacyn® are also included for comparison. *, $p < 0.05$.

Figure 6 shows the texture profile for topical treatments prepared with 1.5% (w/v) gelatin. As in the previous case, the hardness shows no recognizable trend, ending the 28 days of age with a decrease of about 50% with respect to the fresh sample. Compressibility also starts very high with values between 50-60 N.mm but decreases steadily to values below 10 N.mm by the end of the entire aging period. For the same period, adhesiveness also drops drastically from values between 20-25 N.mm to values below 2 N.mm, showing better results at higher PVA concentrations. Finally, except for the 0.7% (w/v) PVA, cohesiveness showed a decreasing trend reaching relatively stable values after seven days of aging. The commercial treatments show no significant changes at any of the evaluated time points during the entire accelerated aging period [93, 97, 98, 99].

The texture profile parameters of the formulations must be balanced to achieve the needs of topical use. For example, low hardness and compressibility are desired to prolong their contact time with the affected skin area. This is critical to avoid any detrimental impact on the newly formed skin cells while maintaining sufficient consistency [100]. In addition, it is important to prevent excessive adhesion to the surface as this could hinder the diffusion of the treatment towards the bacterial biofilm [98]. Therefore, according to Figure 5 and Figure 6 and based on intermediate-low hardness and compressibility, low adhesiveness, intermediate cohesiveness, and lower variability of textural properties, it was decided to choose the formulations of 1.1% and 1.5% (w/v) gelatin with 0.7% (w/v) PVA to proceed with the encapsulation of GO-Ag NP.

Figure 7 shows the texture profile analysis for the topical treatments as they were subjected to aging in the presence and absence of the GO-Ag NP. The nanocomposite hydrogels showed about the same hardness after completing the aging study. This was not the case for the treatments in the absence of the nanoconjugates, where it was declining markedly. Also, the presence of the nanoconjugates led to an increase in hardness stability after aging, especially for the formulations with 1.5% (w/v) gelatin concentration. Compressibility during the first 14 days was similar for the formulations in the presence and absence of the nanoconjugates, especially the treatment with 1.1% (w/v) gelatin. However, at the end of the aging test, a statistically significant difference was found for the 1.5% (w/v) treatment, which showed an increase of 350% with respect to the formulation in the absence of the nanoconjugates. As for hardness, a lower variability over time was observed, which would indicate greater stability. When looking at the adhesiveness of the nanocomposite hydrogels, it can be observed that during the first 14 days, the behavior is similar to that of the treatment with 1.1% (w/v) gelatin in the absence of the nanoconjugates. After 28 days, it is observed that the degradation continues, leading to adhesiveness values below 1.5 N.mm. This suggests that including the nanoconjugate in the formulation results in no alteration of the formulation adhesiveness at the end of the aging study compared with the pristine hydrogel. The cohesiveness exhibited by the topical formulations in the presence of the nanoconjugates from baseline and after 14 days of aging was lower than that in the absence of the nanoconjugates. Notably, after the aging study, the cohesiveness of the nanocomposite hydrogels was significantly higher than that of pristine formulations. Moreover, they showed an almost perfectly elastic behavior, given that cohesiveness is close to 1.0 [44], which is an attribute needed for patient administration [64]. These results agree with the obtained rheological data as evidenced by Figure 3 on both G' and viscosity for the 0.7% (w/v) gelatin hydrogels (see **Figure S 7**), in the sense that the degradation is higher for formulations prepared at such gelatin concentration. Moreover, the presence of the nanoconjugates in the formulation help maintain properties about constant over time.

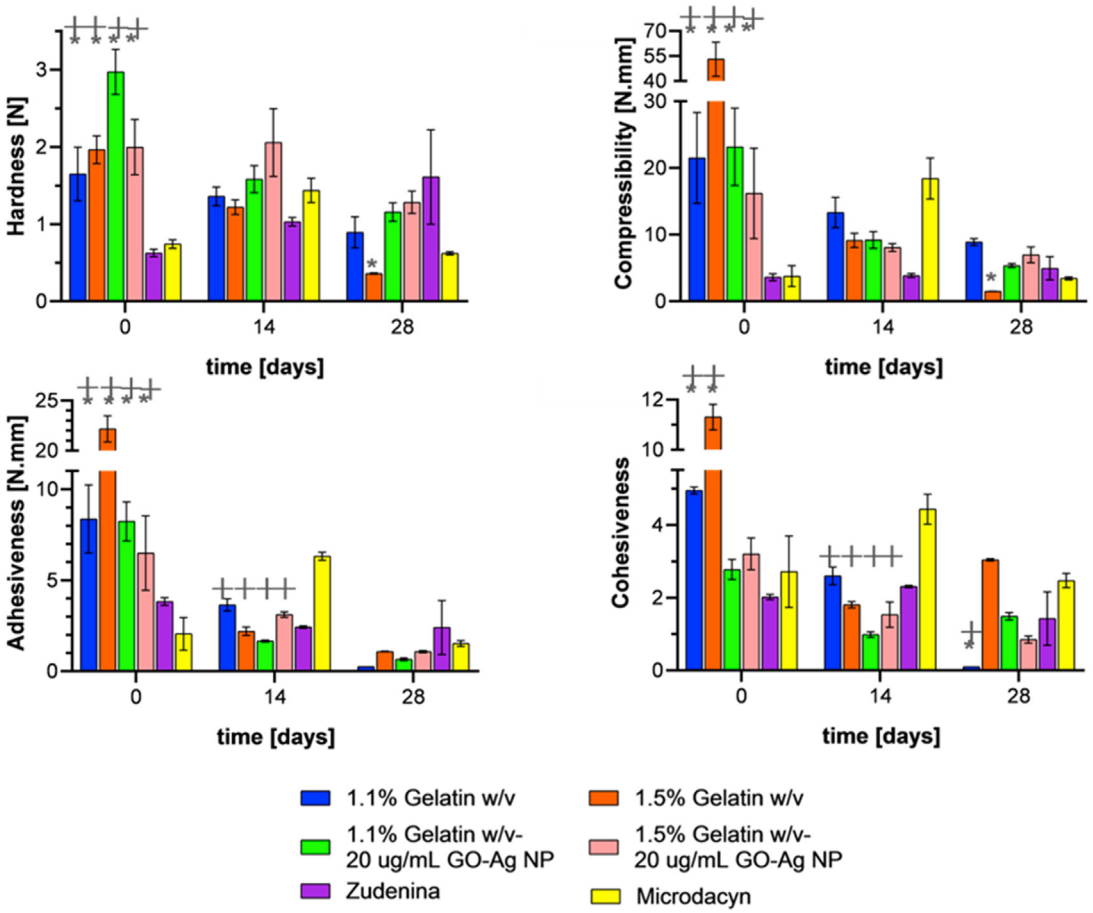

Figure 7. Texture profile analysis for freshly prepared hydrogels with presence and absence of GO-Ag NPs and evaluated at 14 and 28 days of exposure to accelerated aging conditions at 40 °C and 75% RH. *, $p < 0.05$.

3.5. Particle size determination

Particle size distribution analysis of the topical treatments in Figure 8 A and B and **Figure S 8** A and B for freshly prepared hydrogels showed multimodal distributions peaking predominantly between 600-800 μm. This might be due to the presence of polymeric chains of gelatin, PVA, Carbopol®, and hyaluronic acid with different molecular weights. As the chains interact under shear stress, they can form structures or aggregates of varying sizes [101, 102]. A much less abundant proportion of particles was detected in the range between 10-300 μm, indicating that shorter chains were less prevalent in the starting polymeric blend. Independent of the multimodality obtained, the dominant particle size ranges have been reported to be well suited for drug delivery and encapsulation purposes [103]. No apparent concentration-dependent trend is observed, but the freshly prepared formulations exhibited similar behavior.

In contrast with our formulations, Zudenina® showed much smaller particle sizes (between 0.1 and 10 μm) due to the presence of two microparticulate antibiotics and Carbopol® (according to the formulation presented in the packaging box). A small peak was also identified at around 800 μm, attributed to the thickening polymer [63]. Microdacyn® offers a monodisperse distribution mainly due to the simplicity of its formulation that is principally based on hypochlorous acid. According to **Figure S 9**, the volume-weighted diameter of the hydrogels prepared with 1.1% and 1.5% (w/v) gelatin showed only a 10–20% reduction after completing the accelerated aging test. This indicates that agglomeration processes are largely avoided even in the presence of the nanoconjugates [104]. Somewhat surprisingly, at the end of the aging month, the topical treatments showed narrower and much sharper monodisperse distributions [105]. Similar results were found for Microdacyn®, which showed a very sharp distribution (at around 800 μm) towards the end of the aging test month. On the contrary, Zudenina® presents a decrease in its volume-weighted diameter distribution after the aging test, losing such a peak.

Figure 9 shows that for the 1.1% (w/v) gelatin in the presence of the nanoconjugate, the distribution peaks at a higher value than the freshly prepared hydrogel. This may be related to the reinforcement of the polymeric matrix [106]. After 28 days, there is no difference with the pristine hydrogel, and the level of degradation is comparable. In the case of 1.5% (w/v) gelatin, no difference was observed between the freshly prepared hydrogels in the presence or absence of the nanoconjugates. In this case, degradation occurs after 28 days, shifting the distribution peak towards smaller particle sizes and making it sharper. The addition of the nanoconjugates to the blend appears not to induce any further agglomeration. This might be due to superior interactions of the nanoconjugates with the nitrogen and oxygen atoms and carboxylate anions along the main backbones of the polymeric components [106, 107].

3.6. Stability profiles

Figure 10 presents the Turbiscan stability index (TSI), which considers all processes taking place within the sample (sedimentation, clarification, and coalescence) [108]. The higher the TSI value, the more unstable the topical treatment is. This parameter was evaluated during 33 days under accelerated aging conditions, which showed different processes depending on the formulation of the topical treatment. In the case of the 0.7% (w/v) gelatin, the lowest TSI was obtained mainly due to its translucent appearance. However, with the passing of the days, these formulations lost their structural integrity and even liquefied, as

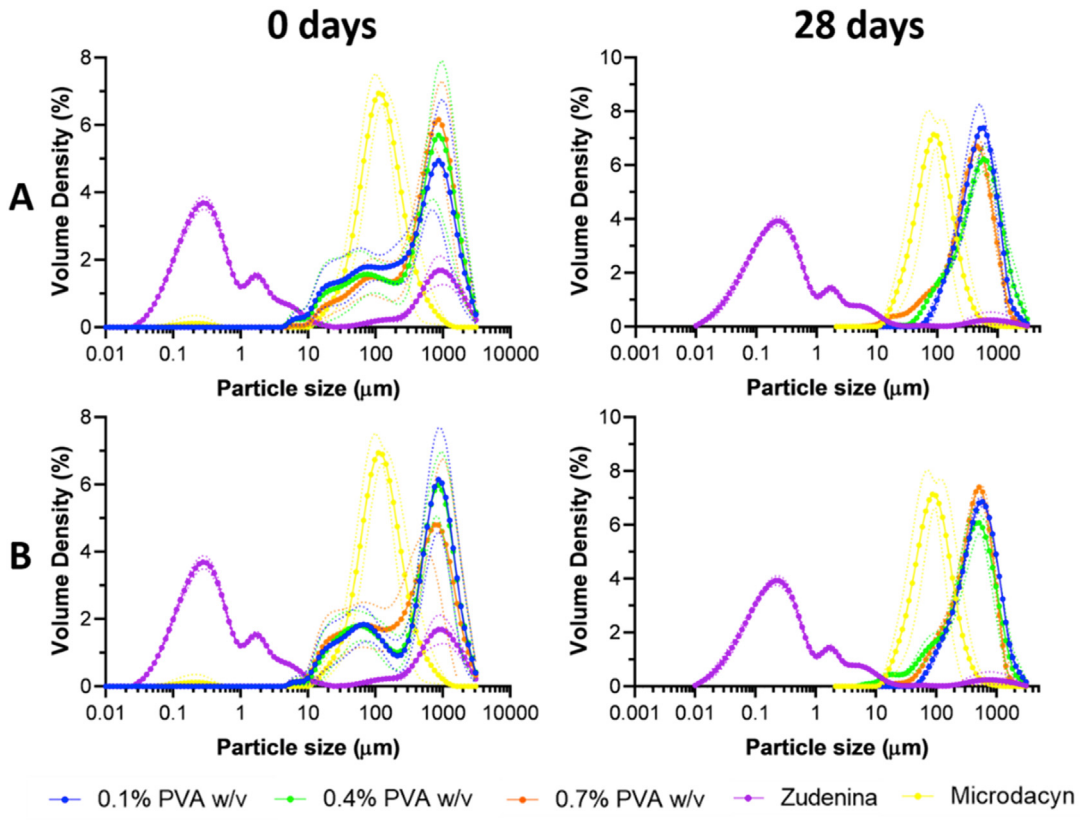

Figure 8. Particle size distribution for hydrogels at 1.1% (w/v) gelatin (**A**) and 1.5% (w/v) gelatin (**B**) freshly prepared and evaluated at 28 days exposure to accelerated aging conditions at 40 °C and 75% RH. Commercial treatments Zudenina® and Microdacyn® are also included for comparison.

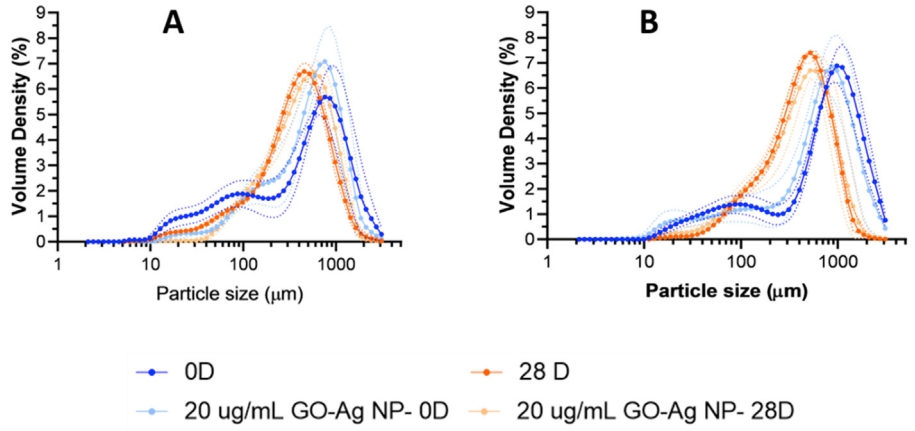

Figure 9. Particle size distribution for hydrogels with 0.7% (w/v) PVA, 20 μg/mL GO-Ag NPs, 1.1% (w/v) gelatin (**A**) and 1.5% (w/v) gelatin (**B**) freshly prepared and evaluated at 28 days exposure to accelerated aging conditions at 40 °C and 75% RH.

evidenced in the rheological behavior. They also show the greatest variability due to insufficient crosslinking, greater mobility of the polymer chains, and molecular disorder due to aging. Even though the 1.1% and 1.5% (w/v) gelatin formulations tend to destabilize more, crosslinking tends to prevent such processes, as was observed for high concentrations of PVA [109, 110]. Importantly, the collected data showed low variability and constant TSI values at high PVA concentrations after 7–10 days of aging. The commercially available Zudenina® showed superior stability and maintained its TSI below 0.5 throughout the aging study. This is in complete agreement with the results of rheological behavior. In contrast, Microdacyn® showed visual evidence of phase separation, which failed to correlate with the TSI since it ended the aging study with a value of 12.

For the nanocomposite hydrogels, it was observed that the TSI of the 1.5% (w/v) gelatin improved drastically from 70 to 8 as described previously by Sun et al. in a similar study [111]. In contrast, for the 1.1% (w/v) gelatin, the inclusion of the GO-Ag NPs nanoconjugate tends to favor increased stability during the first two weeks of aging. Still, at the end of the test, no significant differences were identified with respect to the pristine material. This behavior would indicate a strong interaction between the gelatin polymeric chain and the nanoconjugate, which, at a greater proportion, would facilitate the physical stabilization of the

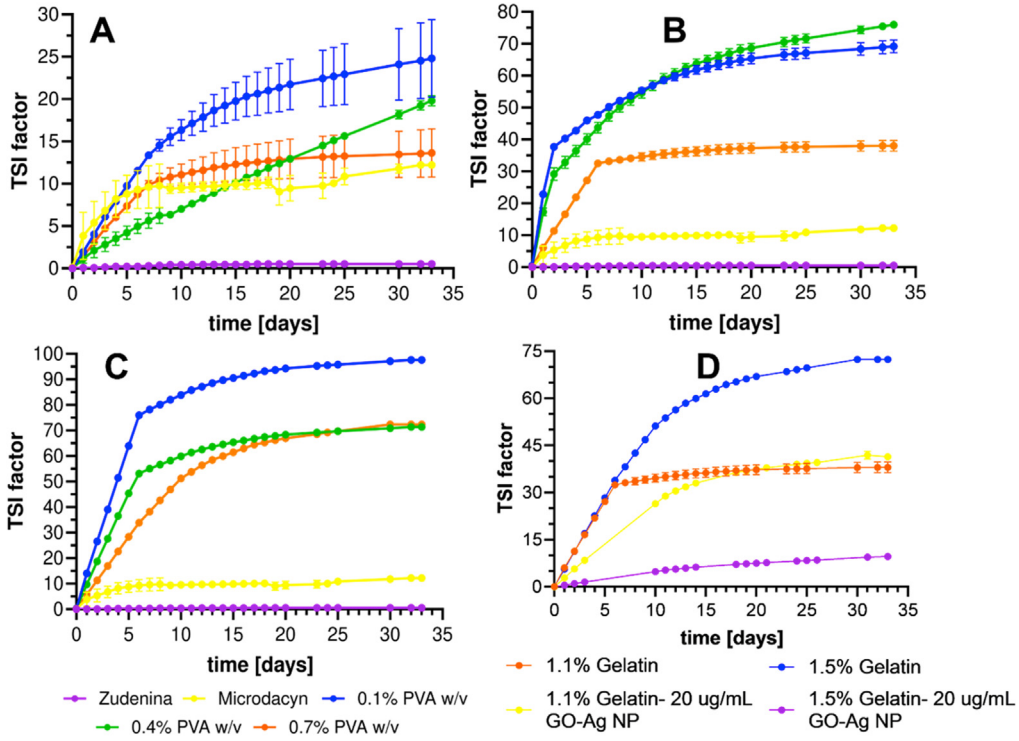

Figure 10. Destabilization kinetics for topical treatments based on Turbiscan stability index (TSI) factor for hydrogels with 0.7% (w/v) gelatin (**A**), 1.1% (w/v) gelatin (**B**), and 1.5% (w/v) gelatin (**C**) evaluated during 33 days of exposure to accelerated aging conditions at 40 °C and 75% RH. In addition, the treatment for hydrogels with GO-Ag NPs is shown (**D**).

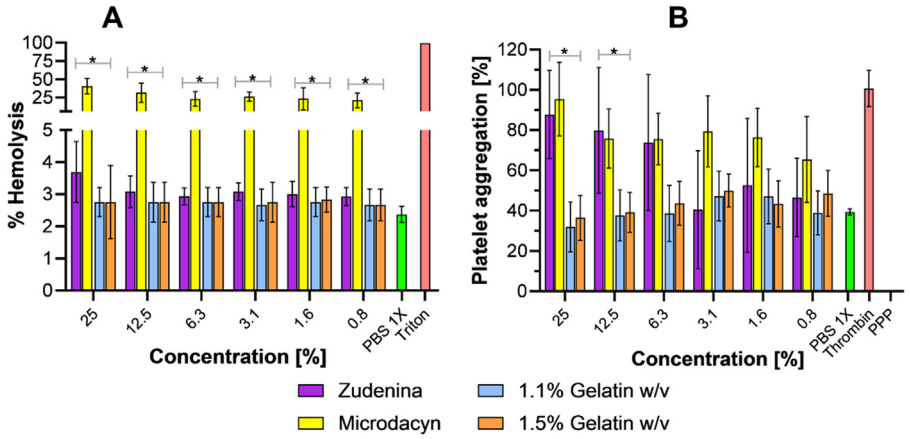

Figure 11. Hemolytic effect (**A**) and platelet aggregating capacity (**B**) for the treatments with 0.7% (w/v) PVA, 20 μg/mL GO-Ag NPs. In addition, commercial treatments also were evaluated. *, $p < 0.05$.

topical treatment. The aging test showed that destabilization kinetics of formulations in the presence of GO-Ag NPs nanoconjugates (Figure 10 D) is superior to that of pristine materials, as evidenced by higher TSI values. However, the resilience of the nanocomposites appears responsible for slowing down processes such as coalescence or sedimentation [110, 112].

3.7. Hemolysis assay

This biocompatibility assay conducted *in vitro* is important to estimate whether hemolysis is induced if, by chance, the topical formulation comes in contact with blood. Figure 11 A shows that the developed topical treatments cause the same level of hemolysis of the negative control, which was below 5% in all cases. Similar results were obtained with Zudenina®. However, Microdacyn® showed a hemolytic effect between 25 and 50% for the different concentrations evaluated. This experiment allowed us to conclude that our nanocomposite hydrogels have high hemocompatibility [113, 114, 115, 116].

3.8. Platelet aggregation assay

Figure 11 B shows the platelet aggregating capacity of our topical hydrogel formulations and the commercially available ones. The results suggest that the nanocomposite hydrogels with 1.1% and 1.5% (w/v) gelatin have a moderate to low platelet aggregating capacity (at the same level of the negative control), which might be helpful for regeneration purposes. This might be attributed to the collagen present in the polymeric blend, as it has been reported previously as a biomaterial capable

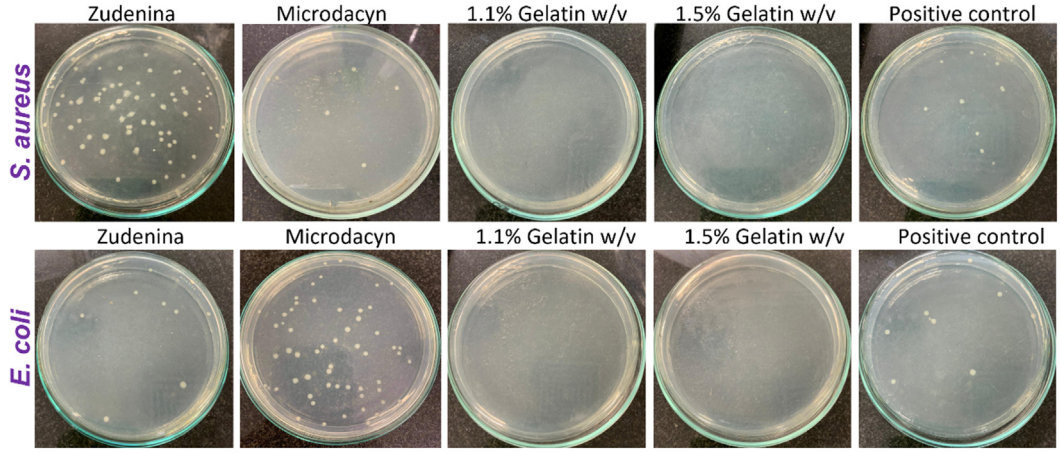

Figure 12. Representative photos of bacteria colonies counting on Mueller-Hinton agar plates after 18h incubation at 37 °C and exposed to our topical formulations with 1.1% and 1.5% (w/v) gelatin with 0.7% (w/v) PVA and 20 μg/mL GO-Ag NPs, the commercial treatments, and the positive control (n = 15).

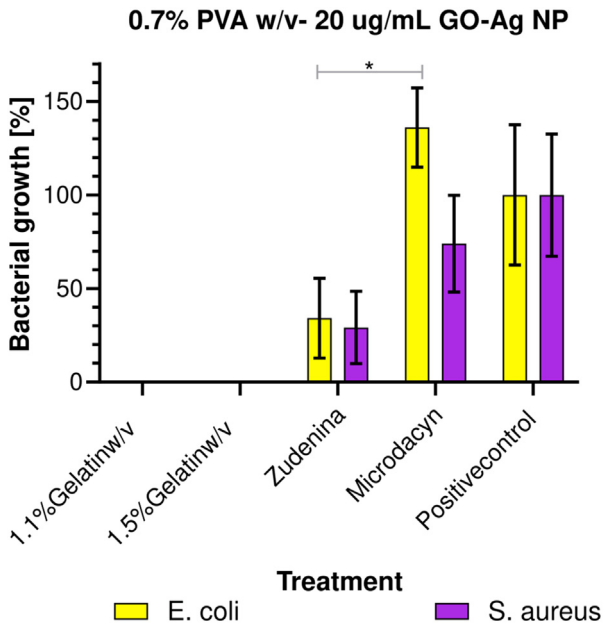

Figure 13. Bacterial growth for the 1.1% and 1.5% (w/v) gelatin with 0.7% (w/v) PVA and 20 μg/mL GO-Ag NPs treatment, the commercial treatments, and the positive control (n = 15). *, $p < 0.05$.

of adhering platelets to its surface and facilitating aggregation and degranulation to form clots [117]. This also allowed us to infer that the macrostructure of gelatin is likely retained to a large extent in our formulations. This result adds up to the promissory list of attributes of the prepared formulations and even the possibility of extending it for additional applications such as wound dressing and bleeding arrest devices for patients with coagulation disorders [118, 119, 120, 121]. Zudenina® and Microdacyn® showed a superior platelet aggregating capacity, which even approached the positive control; however, the results also indicate that as their concentration decreases, the platelet aggregating capacity slightly declines.

3.9. Topical treatments antimicrobial activity

Figure 12 shows the bacterial colony count (quintuplicate) in Mueller Hinton agar plates for the different formulations. In this regard, our topical nanocomposite hydrogel treatments with 1.1% and 1.5% (w/v) gelatin showed high antimicrobial activity, evidenced by a 100% reduction in bacterial growth. This is a satisfactory performance considering the exceedingly low dose of the nanoconjugate required (i.e., 20 μg/mL). These results align well with the already demonstrated antibacterial activity of PVA, which would increase even further by the presence of the GO-Ag NPs nanoconjugates within the polymeric blend [87]. This activity was statistically different with respect to the commercial treatments and the positive control (see Figure 13). The antibacterial mechanism is likely related to the ability of AgNPs to disrupt bacterial cell walls and/or internalize cells to induce permanent damage of the intracellular machinery and, in turn, cause cell death [48, 60, 94]. Zudenina® and Microdacyn® showed a much less effective reduction of bacterial growth for Gram-positive and Gram-negative strains.

Figure 13 shows the calculated bacterial growth percentage for all topical formulations and the commercial controls [122]. As described above, our formulations eliminated 100% of bacteria. However, Zudenina® eliminated about 50% of *S. aureus* and *E. coli*. In comparison, Microdacyn® failed to eliminate *E. coli* and only about 30% of *S. aureus* without a statistically significant difference with respect to the positive control. The inefficacy of these commercially available products might be related to the limited shelf-life of the active compounds or instability issues.

Our results hold much promise as they prove the high quality of the developed topical treatments against *E. coli* and *S. aureus,* responsible for severe healthcare-associated infections (HAI) [123]. Moreover, they open the possibility for further engineering the materials to incorporate additional excipients such as anti-inflammatory or immunomodulatory compounds for addressing more comprehensively wound healing [124].

3.10. Evaluation of cell viability via MTT assay

Figure 14 shows the cell viability percentage of Vero cells after 24 and 48 h of exposure to the extracts of 1.1% and 1.5% (w/v) Gelatin – 20 ug/mL GO-Ag NPs hydrogels. Results show high biocompatibility (viability above 80%) at concentrations below 12.5% (v/v). However, at a concentration above 12.5% (v/v), the extracts led to cytotoxicity that increased in a concentration-dependent manner. This behavior can be related to the increase in the concentration of GO-Ag nanocomposites due to an increase in the concentration of the extracts. In addition, the extracts of 1.1% (w/v) Gelatin – 20 μg/mL GO-Ag NPs hydrogel exposed higher toxicity than extracts of 1.5% (w/v) Gelatin hydrogel. This tendency can be related to a decrease in the release rate of GO-Ag NPs. The gelatin concentration impacts the nanocomposites' encapsulation efficiency and, therefore, the release rate. These results confirm the high biocompatibility of the hydrogels at middle to low concentrations,

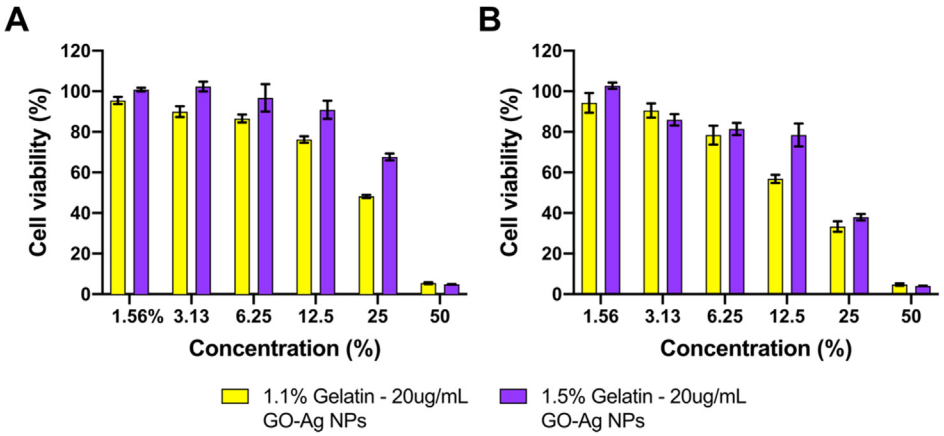

Figure 14. Cell viability of Vero cells for extracts of 1.1% and 1.5% (w/v) Gelatin – 20 μg/mL GO-Ag NPs. Cell viability after 24 (**A**) and 48 h (**B**) of exposure.

suggesting their applicability as a promising antimicrobial topical treatment with low impact on healthy cells.

4. Conclusions

In this work, we synthesized, characterized, and evaluated physicochemically and biologically topical antibacterial treatments based on a polymeric gelatin-polyvinyl alcohol network loaded with antimicrobial GO-Ag NPs nanoconjugates and compared them with commercially available formulations. The antibacterial activity of the formulations prepared at 20 μg/mL was remarkable, as evidenced by 100% inhibition of bacterial growth for *E. Coli* and *S. aureus*. Moreover, the treatment showed high biocompatibility and a marked pseudoplastic rheological behavior. Taken together, these results hold much promise and encourage us to investigate their performance further prior to reaching in vivo and clinical studies. For instance, it would be desirable to extend the aging study instead of considering accelerated conditions under real-time constraints for at least six months.

Additionally, we believe that it is vital to evaluate the biological response of the topical treatments after accelerated and real-time aging periods. This should be accompanied by a precise determination of the minimum inhibitory concentration and an evaluation of potency against resistant bacterial strains. Finally, it would be worth testing the topicals *in vitro* using infected organotypic skin models and *ex vivo* in an infected porcine skin model.

Informed consent statement

Informed consent was obtained from all blood donors involved in the study.

Declarations

Author contribution statement

Jorge Luis Patarroyo; Javier Cifuentes: Conceived and designed the experiments; Performed the experiments; Analyzed and interpreted the data; Wrote the paper.

Laura N. Muñoz: Performed the experiments.

Juan C. Cruz; Luis H. Reyes: Conceived and designed the experiments; Analyzed and interpreted the data; Contributed reagents, materials, analysis tools or data; Wrote the paper.

Funding statement

This work was supported by the Colombian Ministry of Science, Technology, and Innovation (Minciencias), Grants ID 120484467244.

Data availability statement

Data included in article/supplementary material/referenced in article.

Declaration of interests statement

The authors declare no conflict of interest.

Additional information

Supplementary content related to this article has been published online at https://doi.org/10.1016/j.heliyon.2022.e09145.

Acknowledgements

Chemical and Food Engineering Department, Biomedical Engineering Department, and Microscopy Center at Universidad de los Andes.

References

[1] Q. Bo, et al., Decellularized dermal matrix-based photo-crosslinking hydrogels as a platform for delivery of adipose derived stem cells to accelerate cutaneous wound healing, Mater. Des. 196 (2020) 1–11.
[2] P. Li, et al., Low-drug resistance carbon quantum dots decorated injectable self-healing hydrogel with potent antibiofilm property and cutaneous wound healing, Chem. Eng. J. 403 (May 2020) (2021).
[3] K. Wang, et al., Synthesis of a novel anti-freezing, non-drying antibacterial hydrogel dressing by one-pot method, Chem. Eng. J. 372 (2019) 216–225.
[4] C.M. González-Henríquez, M.A. Sarabia-Vallejos, J. Rodriguez-Hernandez, Advances in the fabrication of antimicrobial hydrogels for biomedical applications, Materials 10 (3) (2017) 1–24.
[5] R.K. Thapa, D.B. Diep, H.H. Tønnesen, Topical antimicrobial peptide formulations for wound healing: current developments and future prospects, Acta Biomater 103 (2020) 52–67.
[6] R. Donlan, J.W. Costerton, Biofilms: survival mechanisms of clinically relevant microorganisms, Clin. Microbiol. Rev. 15 (2) (2002) 167–193.
[7] T.F. Mah, B. Pitts, B. Pellock, G.C. Walker, P.S. Stewart, G.A. O'Toole, A genetic basis for Pseudomonas aeruginosa biofilm antibiotic resistance, Nature 426 (6964) (2003) 306–310.
[8] R.D. Wolcott, et al., Chronic wounds and the medical biofilm paradigm, J. Wound Care 19 (2) (2010) 45–53.
[9] P.R. Puentes, et al., Design , Screening , and Testing of Non-rational Peptide Libraries with Antimicrobial Activity : in Silico and Experimental Approaches, 2020.
[10] B.I. Wounds, M. Nowak, Nanomaterials as a Successor of Antibiotics, 2021.
[11] B. C. Borro, R. Nordström, and M. Malmsten, "Microgels and hydrogels as delivery systems for antimicrobial peptides," Colloids Surf. B Biointerfaces, vol. 187, 2020.
[12] S. Yasasvini, R.S. Anusa, B.N. VedhaHari, P.C. Prabhu, D. RamyaDevi, Topical hydrogel matrix loaded with Simvastatin microparticles for enhanced wound healing activity, Mater. Sci. Eng. C 72 (2017) 160–167.
[13] N. Asadi, H. Pazoki-Toroudi, A.R. Del Bakhshayesh, A. Akbarzadeh, S. Davaran, N. Annabi, Multifunctional hydrogels for wound healing: special focus on biomacromolecular based hydrogels, Int. J. Biol. Macromol. 170 (2021) 728–750.

[14] A. Peptides, et al., Design , synthesis and antifungal activity of stapled Aurein 1.2 peptides, Antibi 10 (2021).
[15] M. Mirzaee, E. Hol, A. Mi, D.J. Kope, Long-Lasting Stable Expression of Human LL-37 Antimicrobial Peptide in Transgenic Barley Plants, 2021, pp. 1–11.
[16] M. Zahoor, et al., A Review on Silver Nanoparticles : Classification , Various Methods of Synthesis , and Their Potential Roles in Biomedical Applications and Water Treatment, 2021, pp. 1–28.
[17] E. Halevas, et al., Evaluation of the Hemocompatibility and Anticancer Potential of Poly (ε -Caprolactone) and Poly (3-Hydroxybutyrate) Microcarriers with Encapsulated Chrysin, 2021.
[18] S. Gunasekaran, K. Thanrasu, A. Manikandan, M. Durka, A. Dinesh, S. Anand, Structural , fabrication and enhanced electromagnetic wave absorption properties of reduced graphene oxide (rGO)/zirconium substituted cobalt ferrite (Co0·5Zr0·5Fe2O4) nanocomposites, Phys. B Phys. Condens. Matter. 605 (December 2020) (2021) 412784.
[19] M. Tabish, et al., Construction of NiCo/graphene nanocomposite coating with bulges-like morphology for enhanced mechanical properties and corrosion resistance performance, J. Alloys Compd. 867 (2021) 159138.
[20] G. Yasin, et al., Revealing the erosion-corrosion performance of sphere-shaped morphology of nickel matrix nanocomposite strengthened with reduced graphene oxide nanoplatelets, Diam. Relat. Mater. 104 (February) (2020) 107763.
[21] Y.S. Sadeeq Ullah, Ghulam Yasin, Aftab Ahmad, Lei Qin, Qipeng Yuan, Arif Ullah Khan, Usman Ali Khan, Aziz Ur Rahman, Construction of well-designed 1D selenium-tellurium nanorods anchored on graphene sheets as high storage capacity anode material in lithium-ion battery, Inorg. Chem. Front. 7 (2020) 1750–1761.
[22] G. Yasin, M. Arif, T. Mehtab, M. Shakeel, A novel strategy for the synthesis of hard carbon spheres encapsulated with graphene networks as a low-cost and large-scalable anode material for fast sodium storage with an ultralong cycle life, Inorg. Chem. Front. 7 (2019) 402–410.
[23] S. Akhtar, S. Rehman, M.A. Almessiere, F.A. Khan, Nanoparticles via the hydrothermal approach induced anti-cancer and anti-bacterial activities, Nanomaterials 1635 (2019) 1–12.
[24] S.E. Shirsath, A. Baykal, Synthesis of Dy-Y co-substituted manganese - zinc spinel nanoferrites induced anti-bacterial and anti-cancer activities : comparison between sonochemical and sol-gel auto-combustion methods, Mater. Sci. Eng. C 116 (1982) (2020) 111186.
[25] G. Bacteria, et al., Synthesis of electrospun TiO 2 nanofibers and characterization of their antibacterial and antibiofilm potential against gram-positive and gram-negative bacteria, Antibiotics 9 (572) (2020).
[26] A. Shokry, M. Khalil, H. Ibrahim, M. Soliman, S. Ebrahim, Acute toxicity assessment of polyaniline/Ag nanoparticles/graphene oxide quantum dots on Cypridopsis vidua and Artemia salina, Sci. Rep. 11 (1) (2021) 1–10.
[27] X.W. Han, H. Pan, M. Liu, In situ green growth of uniform and naked Ag nanoparticles on graphene oxide at room temperature and its enhanced catalytic performance, J. Nanoparticle Res. 22 (6) (2020).
[28] K. Prakash, D.T. Masram, Silver Nanoparticles Immobilized Covalent Organic Microspheres for Hydrogenation of Nitroaromatics with Intriguing Catalytic Activity, 2020.
[29] H.M. Mcintyre, M.L. Hart, Immobilization of TiO 2 Nanoparticles in Cement for Improved Photocatalytic Reactivity and Treatment of Organic Pollutants, 2021.
[30] I. V Korolkov, et al., Boron and Gadolinium Loaded Fe 3 O 4 Nanocarriers for Potential Application in Neutron Cancer Therapy, 2021.
[31] K. Chaudhary, K. Prakash, D.T. Masram, TiO 2 nanoparticles immobilized organo-reduced graphene oxide hybrid nanoreactor for catalytic applications, Appl. Surf. Sci. 509 (November 2019) (2020) 144902.
[32] S.K.A. Deepika Yadav, Pd NPs confined novel covalent organic polymer for catalytic application, New J. Chem. 44 (2020) 1320–1325.
[33] R. Szcz, T.K.A. Hoang, L. Dobrza, Solution/Ammonolysis Syntheses of Unsupported and no. I, 2021.
[34] B.D. Mansuriya, Z. Altintas, Enzyme-Free Electrochemical Nano-Immunosensor Based on Graphene Quantum Dots and Gold Nanoparticles for Cardiac Biomarker Determination, 2021.
[35] N.K. Mogha, K. Chaudhary, G. Kumar, D.T. Masram, Fur-Imine-Functionalized graphene oxide-immobilized copper oxide nanoparticle catalyst for the synthesis of xanthene derivatives, ACS Omega 3 (2018) 16377–16385.
[36] D.I. Rodríguez-otamendi, et al., Eco-friendly synthesis of graphene oxide – silver nanoparticles hybrids : the effect of amine derivatization, Diam. Relat. Mater. 111 (108208) (2021).
[37] S. Pipattanachat, J. Qin, D. Rokaya, P. Thanyasrisung, Biofilm inhibition and bactericidal activity of NiTi alloy coated with graphene oxide/silver nanoparticles via electrophoretic deposition, Sci. Rep. (2021) 1–10.
[38] H. Liu, C. Hao, Y. Zhang, H. Yang, R. Sun, The interaction of graphene oxide-silver nanoparticles with trypsin: insights from adsorption behaviors, conformational structure and enzymatic activity investigations, Colloids Surf. B Biointerfaces 202 (February) (2021) 111688.
[39] L. Zhang, Y. Yu, S. Zheng, L. Zhong, J. Xue, Preparation and Properties of Conductive Bacterial Cellulose-Based Graphene Oxide-Silver Nanoparticles Antibacterial Dressing 257, 2021. January.
[40] U. Piotrowska, M. Sobczak, E. Oledzka, Current state of a dual behaviour of antimicrobial peptides—therapeutic agents and promising delivery vectors, Chem. Biol. Drug Des. 90 (6) (2017) 1079–1093.
[41] H. Kitagawa, et al., Development of sustained antimicrobial-release systems using poly(2-hydroxyethyl methacrylate)/trimethylolpropane trimethacrylate hydrogels, Acta Biomater 10 (10) (2014) 4285–4295.
[42] D. Singh, M.R. Singh, Development of antibiotic and debriding enzyme-loaded PLGA microspheres entrapped in PVA-gelatin hydrogel for complete wound management, Artif. Cell Blood Substit. Biotechnol. 40 (5) (2012) 345–353.
[43] F. Davoodi-Roodbordeii, et al., Topical hydrogel containing Fumaria vaillantii Loisel. extract enhances wound healing in rats, BMC Compl. Alternative Med. 19 (1) (2019) 1–9.
[44] N.T. Tung, V.D. Vu, P.L. Nguyen, DoE-based development, physicochemical characterization, and pharmacological evaluation of a topical hydrogel containing betamethasone dipropionate microemulsion, Colloids Surf. B Biointerfaces 181 (March) (2019) 480–488.
[45] M. Bustamante-torres, V.H. Pino-ramos, D. Romero-fierro, S.P. Hidalgo-bonilla, H. Magaña, E. Bucio, Synthesis and Antimicrobial Properties of Highly Cross-Linked pH-Sensitive Hydrogels through Gamma Radiation, 2021, pp. 1–16.
[46] H. Fang, et al., A novel high-strength poly(ionic liquid)/PVA hydrogel dressing for antibacterial applications, Chem. Eng. J. 365 (2019) 153–164.
[47] F.M. Croisfelt, et al., Modified-release topical hydrogels: a ten-year review, J. Mater. Sci. 54 (16) (2019) 10963–10983.
[48] D.M. Júnior, et al., A new dermal substitute containing polyvinyl alcohol with silver nanoparticles and collagen with hyaluronic acid: in vitro and in vivo approaches, Antibiotics 10 (6) (2021) 742.
[49] D. Li, Y. Ye, D. Li, X. Li, C. Mu, Biological properties of dialdehyde carboxymethyl cellulose crosslinked gelatin-PEG composite hydrogel fibers for wound dressings, Carbohydr. Polym. 137 (2016) 508–514.
[50] H. Tan, D. Huang, L. Lao, C. Gao, RGD modified PLGA/gelatin microspheres as microcarriers for chondrocyte delivery, J. Biomed. Mater. Res. B Appl. Biomater. 91 (1) (2009) 228–238.
[51] I. Lequeux, E. Ducasse, T. Jouenne, P. Thebault, Addition of antimicrobial properties to hyaluronic acid by grafting of antimicrobial peptide, Eur. Polym. J. 51 (1) (2014) 182–190.
[52] J. Zhu, X. Tang, Y. Jia, C. T. Ho, and Q. Huang, "Applications and delivery mechanisms of hyaluronic acid used for topical/transdermal delivery – a review," Int. J. Pharm., vol. 578, no. September 2019, 2020.
[53] S.G. Lee, et al., Enhanced topical delivery of tacrolimus by a carbomer hydrogel formulation with transcutol P, Drug Dev. Ind. Pharm. 42 (10) (2016) 1636–1642.
[54] J.L. Patarroyo, E. Fonseca, J. Cifuentes, F. Salcedo, J.C. Cruz, L.H. Reyes, Gelatin-graphene oxide nanocomposite hydrogels for kluyveromyces lactis encapsulation: potential applications in probiotics and bioreactor packings, Biomolecules 11 (7) (2021) 922.
[55] D. Philip, Honey mediated green synthesis of silver nanoparticles, Mol. Biomol. Spectrosc. 75 (2010) 1078–1081. Spectrochimica Acta Part A.
[56] G. Laverty, S.P. Gorman, B.F. Gilmore, Antimicrobial peptide incorporated poly(2-hydroxyethyl methacrylate) hydrogels for the prevention of Staphylococcus epidermidis-associated biomaterial infections, J. Biomed. Mater. Res. 100 A (7) (2012) 1803–1814.
[57] K. Pal, A.K. Banthia, D.K. Majumdar, Preparation and characterization of polyvinyl alcohol-gelatin hydrogel membranes for biomedical applications, AAPS PharmSciTech 8 (1) (2007).
[58] E. Alemzadeh, A. Oryan, A.A. Mohammadi, Hyaluronic acid hydrogel loaded by adipose stem cells enhances wound healing by modulating IL-1β, TGF-β1, and bFGF in burn wound model in rat, J. Biomed. Mater. Res. B Appl. Biomater. 108 (2) (2020) 555–567.
[59] J.P. Silva, et al., Improved burn wound healing by the antimicrobial peptide LLKKK18 released from conjugates with dextrin embedded in a carbopol gel, Acta Biomater 26 (2015) 249–262.
[60] R. Singla, et al., Cytocompatible anti-microbial dressings of syzygium cumini cellulose nanocrystals decorated with silver nanoparticles accelerate acute and diabetic wound healing, Sci. Rep. 7 (1) (2017) 1–13.
[61] C.A. Schneider, W.S. Rasband, K.W. Eliceiri, NIH Image to ImageJ: 25 years of image analysis, Nat. Methods 9 (7) (2012) 671–675.
[62] M.A. Gámiz González, U. Edlund, A. Vidaurre, J.L. Gómez Ribelles, Synthesis of highly swellable hydrogels of water-soluble carboxymethyl chitosan and poly(ethylene glycol), Polym. Int. 66 (11) (2017) 1624–1632.
[63] M.T. Islam, N. Rodríguez-Hornedo, S. Ciotti, C. Ackermann, Rheological characterization of topical carbomer gels neutralized to different pH, Pharm. Res. (N. Y.) 21 (7) (2004) 1192–1199.
[64] G. Calixto, A.C. Yoshii, H. Rocha E Silva, B. Stringhetti Ferreira Cury, M. Chorilli, Polyacrylic acid polymers hydrogels intended to topical drug delivery: preparation and characterization, Pharmaceut. Dev. Technol. 20 (4) (2015) 490–496.
[65] A.M. Deliormanlı, M. Türk, Flow behavior and drug release study of injectable pluronic F-127 hydrogels containing bioactive glass and carbon-based nanopowders, J. Inorg. Organomet. Polym. Mater. 30 (4) (2020) 1184–1196.
[66] Q. Wang, H. Zhang, J. Huang, N. Xia, T. Li, Q. Xia, Self-double-emulsifying drug delivery system incorporated in natural hydrogels: a new way for topical application of vitamin C, J. Microencapsul. 35 (1) (2018) 90–101.
[67] A. Mun, H. Simaan Yameen, G. Edelbaum, D. Seliktar, Alginate hydrogel beads embedded with drug-bearing polycaprolactone microspheres for sustained release of paclobutrazol, Sci. Rep. 11 (1) (2021) 1–13.
[68] E. Giuliano, D. Paolino, M.C. Cristiano, M. Fresta, D. Cosco, Rutin-loaded poloxamer 407-based hydrogels for in situ administration: stability profiles and rheological properties, Nanomaterials 10 (6) (2020) 3–5.
[69] Ministerio de Salud y Protección Social, "Resolución No. 3157, Guia para el desarrollo y presentacion de los estudios de estabilidad de medicamentos de síntesis química, Gobierno de Colombia, Bogota, 2018, pp. 1–38.
[70] S. Sengupta, S. Banerjee, B. Sinha, B. Mukherjee, Improved skin penetration using in situ nanoparticulate diclofenac diethylamine in hydrogel systems: in vitro and in vivo studies, AAPS PharmSciTech 17 (2) (2016) 307–317.

[71] International Organization for Standardization, Biological Evaluation of Medical Devices. Selection of Assays for Interactions with Blood, 2017, pp. 1–47.
[72] C. Muñoz-Camargo, et al., Unveiling the multifaceted mechanisms of antibacterial activity of buforin II and frenatin 2.3S peptides from skin micro-organs of the orinoco lime treefrog (Sphaenorhynchus lacteus), Int. J. Mol. Sci. 19 (8) (2018).
[73] C.M. Ramírez-acosta, et al., Ph-responsive, cell-penetrating, core/shell magnetite/silver nanoparticles for the delivery of plasmids: preparation, characterization, and preliminary in vitro evaluation, Pharmaceutics 12 (6) (2020) 1–25.
[74] Clinical and Laboratory Standards Institute, Performance Standards for Antimicrobial Disk Susceptibility Tests 13, 2018.
[75] K. Wang, et al., Novel Nonreleasing Antibacterial Hydrogel Dressing by a One-Pot Method 6, 2020 no. 2.
[76] Z. Bao, et al., Glycol chitosan/oxidized hyaluronic acid hydrogel film for topical ocular delivery of dexamethasone and levofloxacin, Int. J. Biol. Macromol. 167 (2021) 659–666.
[77] H. Ying, et al., In situ formed collagen-hyaluronic acid hydrogel as biomimetic dressing for promoting spontaneous wound healing, Mater. Sci. Eng. C 101 (March) (2019) 487–498.
[78] K. Wang, et al., Novel nonreleasing antibacterial hydrogel dressing by a one-pot method, ACS Biomater. Sci. Eng. 6 (2) (2020) 1259–1268.
[79] S. Li, et al., Self-healing hyaluronic acid hydrogels based on dynamic Schiff base linkages as biomaterials, Carbohydr. Polym. 250 (May) (2020) 1–9.
[80] S. Zhang, et al., Arginine derivatives assist dopamine-hyaluronic acid hybrid hydrogels to have enhanced antioxidant activity for wound healing, Chem. Eng. J. 392 (August 2019) (2020) 1–10.
[81] M.T. Khorasani, A. Joorabloo, H. Adeli, P.B. Milan, M. Amoupour, Enhanced antimicrobial and full-thickness wound healing efficiency of hydrogels loaded with heparinized ZnO nanoparticles: in vitro and in vivo evaluation, Int. J. Biol. Macromol. 166 (2021) 200–212.
[82] R. Sharma, K. Pathak, Polymeric nanosponges as an alternative carrier for improved retention of econazole nitrate onto the skin through topical hydrogel formulation, Pharmaceut. Dev. Technol. 16 (4) (2011) 367–376.
[83] J.L. Patarroyo, J.S. Florez-Rojas, D. Pradilla, J.D. Valderrama-Rincón, J.C. Cruz, L.H. Reyes, Formulation and characterization of gelatin-based hydrogels for the encapsulation of kluyveromyces lactis-Applications in packed-bed reactors and probiotics delivery in humans, Polymers 12 (6) (2020).
[84] P. Chuysinuan, T. Thanyacharoen, K. Thongchai, S. Techasakul, S. Ummartyotin, Preparation of chitosan/hydrolyzed collagen/hyaluronic acid based hydrogel composite with caffeic acid addition, Int. J. Biol. Macromol. 162 (2020) 1937–1943.
[85] K. Shanmugapriya, H. Kim, H.W. Kang, EGFR-conjugated hydrogel accelerates wound healing on ulcer-induced burn wounds by targeting collagen and inflammatory cells using photoimmunomodulatory inhibition, Mater. Sci. Eng. C 118 (September 2020) (2021).
[86] H. Ding, D. Nie, N. Cui, K. Li, X. Zhang, L. Zhang, Catalytic reduction of organic dyes by multilayered graphene platelets and silver nanoparticles in polyacrylic acid hydrogel, Materials 14 (9) (2021) 1–13.
[87] I. Gholamali, M. Asnaashariisfahani, E. Alipour, Silver nanoparticles incorporated in pH-sensitive nanocomposite hydrogels based on carboxymethyl chitosan-poly (vinyl alcohol) for use in a drug delivery system, Regen. Eng. Transl. Med. 6 (2) (2020) 138–153.
[88] R. Sahraei, M. Ghaemy, Synthesis of modified gum tragacanth/graphene oxide composite hydrogel for heavy metal ions removal and preparation of silver nanocomposite for antibacterial activity, Carbohydr. Polym. 157 (2017) 823–833.
[89] T.C. dos Santos, et al., Nanocomposite chitosan hydrogels based on PLGA nanoparticles as potential biomedical materials, Eur. Polym. J. 99 (October 2017) (2018) 456–463.
[90] W. Shao, X. Liu, H. Min, G. Dong, Q. Feng, S. Zuo, Preparation, Characterization, and Antibacterial Activity of Silver Nanoparticle-Decorated Graphene Oxide Nanocomposite, 2015.
[91] R. Zhao, et al., Highly Stable Graphene-Based Nanocomposite (GO – PEI – Ag) with Broad-Spectrum , Long-Term Antimicrobial Activity and Antibio Fi Lm E Ff Ects, 2018.
[92] S. Khorrami, Z. Abdollahi, G. Eshaghi, A. Khosravi, An improved method for fabrication of Ag-GO nanocomposite with controlled anti-cancer and anti-bacterial behavior; A Comparative Study, 2019, pp. 1–10. December 2018.
[93] C.C. Kuo, H. Qin, Y. Cheng, X. Jiang, X. Shi, An integrated manufacturing strategy to fabricate delivery system using gelatin/alginate hybrid hydrogels: 3D printing and freeze-drying, Food Hydrocolloids 111 (August 2020) (2021).
[94] M. Ragothaman, A. Kannan, A. Dhanasekaran, Bio-hybrid hydrogel comprising collagen-capped silver nanoparticles and melatonin for accelerated tissue regeneration in skin defects, Mater. Sci. Eng. C 128 (July) (2021) 112328.
[95] C. Ferrag, et al., Polyacrylamide hydrogels doped with different shapes of silver nanoparticles: antibacterial and mechanical properties, Colloids Surf. B Biointerfaces 197 (July 2020) (2021) 111397.
[96] S.H. Park, J.Y. Park, Y.B. Ji, H.J. Ju, B.H. Min, M.S. Kim, An injectable click-crosslinked hyaluronic acid hydrogel modified with a BMP-2 mimetic peptide as a bone tissue engineering scaffold, Acta Biomater 117 (2020) 108–120.
[97] ChanglingWu, D.J. McClements, M. He, Z. Fan, Y. Li, F. Teng, Preparation of okara cellulose hydrogels using ionic liquids: structure, properties, and performance, J. Mol. Liq. 331 (2021).
[98] V.G.R. Patlolla, W.P. Holbrook, S. Gizurarson, P. Kristmundsdottir, Evaluation of in vitro mucoadhesiveness and texture profile analysis of doxycycline in situ hydrogels, Pharmazie 75 (1) (2020) 7–12.
[99] X. Liu, J. Gan, S. Nirasawa, E. Tatsumi, L. Yin, Y. Cheng, Effects of sodium carbonate and potassium carbonate on colloidal properties and molecular characteristics of konjac glucomannan hydrogels, Int. J. Biol. Macromol. 117 (2018) 863–869.
[100] N.A. Mohd Razali, W.C. Lin, Textural and tensile properties of thermo-responsive poly(2-(2-methoxyethoxy)ethyl methacrylate) hydrogel, Mater. Sci. Technol. 35 (14) (2019) 1742–1748.
[101] G. Mancini, et al., Increased Therapeutic Efficacy of SLN Containing Etofenamate and Ibuprofen in Topical Treatment of Inflammation, 2021.
[102] A. Atipairin, C. Chunhachaichana, and T. Nakpheng, "Development of a Sildenafil Citrate Microemulsion-Loaded Hydrogel as a Potential System for Drug Delivery to the Penis and its Cellular Metabolic Mechanism," vol. 5, pp. 1–23.
[103] J.D.C. Candido, et al., Alginate hydrogels incorporating neomycin or propolis as potential dressings for diabetic ulcers: structure, swelling, and antimicrobial barrier properties, Polym. Adv. Technol. 30 (10) (2019) 2623–2635.
[104] R.P. Gazzi, L.A. Frank, G. Onzi, A.R. Pohlmann, S.S. Guterres, New pectin-based hydrogel containing imiquimod-loaded polymeric nanocapsules for melanoma treatment, Drug Deliv. Transl. Res. 10 (6) (2020) 1829–1840.
[105] I.N. Pavlova, O.S. Travkina, G.F. Garieva, The influence of hydrogel aging conditions on the crystal size and morphology of LSX zeolite in the NaK-form, Petrol. Chem. 60 (8) (2020) 903–908.
[106] T. Varsha, Y. Murali Mohan, S. Sreedhar, B. Bajpai, Breathing-in/breathing-out approach to preparing nanosilver-loaded hydrogels: highly efficient antibacterial nanocomposites, J. Appl. Polym. Sci. 111 (5) (2009) 934–944.
[107] V. Thomas, M.M. Yallapu, B. Sreedhar, S.K. Bajpai, A versatile strategy to fabricate hydrogel-silver nanocomposites and investigation of their antimicrobial activity, J. Colloid Interface Sci. 315 (1) (2007) 389–395.
[108] W. Jiao, et al., Effects of molecular weight and guluronic acid/mannuronic acid ratio on the rheological behavior and stabilizing property of sodium alginate, Molecules 24 (23) (2019) 1–13.
[109] H. Wang, X. Qin, G. Fei, M. Tian, H. Wen, K. Zhu, Optimization of stability and properties of waterborne polyaniline-graft-poly (vinyl alcohol) nanocomposites with controllable epoxy content, Colloid Polym. Sci. 296 (3) (2018) 585–594.
[110] M. Kowalska, M. Woźniak, A. Krzton-Maziopa, S. Tavernier, Ł. Pazdur, A. Żbikowska, Development of the emulsions containing modified fats formed via enzymatic interesterification catalyzed by specific lipase with various amount of water, J. Dispersion Sci. Technol. 40 (2) (2019) 192–205.
[111] B. Sun, M. Zhang, Y. Ni, Use of sulfated cellulose nanocrystals towards stability enhancement of gelatin-encapsulated tea polyphenols, Cellulose 25 (9) (2018) 5157–5173.
[112] M. Kowalska, A. Krztoń-Maziopa, M. Babut, P. Mitrosz, Rheological and physical analysis of oil-water emulsion based on enzymatic structured fat, Rheol. Acta 59 (10) (2020) 717–726.
[113] D. Zhang, et al., Catechol functionalized chitosan/active peptide microsphere hydrogel for skin wound healing, Int. J. Biol. Macromol. 173 (2021) 591–606.
[114] Y. Pakzad, M. Fathi, Y. Omidi, M. Mozafari, A. Zamanian, Synthesis and characterization of timolol maleate-loaded quaternized chitosan-based thermosensitive hydrogel: a transparent topical ocular delivery system for the treatment of glaucoma, Int. J. Biol. Macromol. 159 (2020) 117–128.
[115] S. Zou, et al., Injectable nanosponge-loaded pluronic f127 hydrogel for pore-forming toxin neutralization, Int. J. Nanomed. 16 (2021) 4239–4250.
[116] M.P. Tian, A. Di Zhang, Y.X. Yao, X.G. Chen, Y. Liu, Mussel-inspired adhesive and polypeptide-based antibacterial thermo-sensitive hydroxybutyl chitosan hydrogel as BMSCs 3D culture matrix for wound healing, Carbohydr. Polym. 261 (February) (2021).
[117] S. Böhm, C. Strauß, S. Stoiber, C. Kasper, V. Charwat, Impact of source and manufacturing of collagen matrices on fibroblast cell growth and platelet aggregation, Materials 10 (9) (2017).
[118] X. Zhang, et al., Berberine-coated biomimetic composite microspheres for simultaneously hemostatic and antibacterial performance, Polymers 13 (3) (2021) 1–16.
[119] J. Qu, X. Zhao, Y. Liang, T. Zhang, P.X. Ma, B. Guo, Antibacterial adhesive injectable hydrogels with rapid self-healing, extensibility and compressibility as wound dressing for joints skin wound healing, Biomaterials 183 (2018) 185–199.
[120] S. Lau, A. Maier, S. Braune, M. Gossen, A. Lendlein, Effect of endothelial culture medium composition on platelet responses to polymeric biomaterials, Int. J. Mol. Sci. 22 (13) (2021).
[121] W. Zieba, J. Czarnecka, T. Rusak, M. Zieba, A.P. Terzyk, Nitric-acid oxidized single-walled carbon nanohorns as a potential material for bio-applications—toxicity and hemocompatibility studies, Materials 14 (6) (2021).
[122] J. Jang, Y. Choi, M. Tanaka, J. Choi, Development of silver/graphene oxide nanocomposites for antibacterial and antibiofilm applications, J. Ind. Eng. Chem. 83 (2020) 46–52.
[123] M. Cobos, I. De-La-Pinta, G. Quindós, M.J. Fernández, M.D. Fernández, Synthesis, physical, mechanical and antibacterial properties of nanocomposites based on poly(vinyl alcohol)/graphene oxide–silver nanoparticles, Polymers 12 (723) (2020) 1–18.
[124] X. Wu, H. Li, N. Xiao, Advancement of Near-infrared (NIR) laser interceded surface enactment of proline functionalized graphene oxide with silver nanoparticles for proficient antibacterial, antifungal and wound recuperating therapy in nursing care in hospitals, J. Photochem. Photobiol. B Biol. 187 (27) (2018) 89–95.